Journal of
Materials Chemistry C

REVIEW

View Article Online
View Journal | View Issue

Published on 18 April 2016. Downloaded by University of Texas Libraries on 14/06/2016 15:37:27.

Cite this: J. Mater. Chem. C, 2016, 4, 5133

Printed photonic elements: nanoimprinting and beyond

Cheng Zhang,[a] Harish Subbaraman,[b] Qiaochu Li,[a] Zeyu Pan,[c] Jong G. Ok,†[a] Tao Ling,[a] Chi-Jui Chung,[c] Xingyu Zhang,[c] Xiaohui Lin,[c] Ray T. Chen[bc] and L. Jay Guo*[a]

Received 25th March 2016,
Accepted 8th April 2016

DOI: 10.1039/c6tc01237j

www.rsc.org/MaterialsC

In order to manufacture large-scale photonic devices of various dimensions at a low cost, a number of patterning techniques have been developed. Nanoimprint lithography is among the most promising given its unique advantages, such as high resolution, fast processing speed, high throughput, compatibility with diverse materials, and low cost. This review covers various aspects of nanoimprint lithography, including its operational principles, material requirements, and different ways of implementation. Nanoimprint lithography facilitates numerous high-performance and low-cost photonic elements, including optical interconnects, sensors, solar cells, and metamaterials. In addition, other related patterning techniques, together with their utilization for photonic device fabrication and their integration with nanoimprint lithography, are briefly discussed.

1. Introduction

Future photonic and optoelectronic devices should be compact in size for high-density on-chip integration. In addition, engineering their configurations at the micro- or nano-scale, *i.e.*, as photonic crystals or metamaterials, can improve their properties and create new device functionalities. These advances demand highly precise techniques to fabricate structures of various sizes using a wide range of materials at low cost and in high throughput.

So far, various microlithography and nanolithography techniques have been developed, many driven by the continuous demands from the semiconductor industry to manufacture smaller transistors and denser integrated circuits. They can be roughly categorized into: (a) photon-based lithography (optical lithography,[1] deep-UV/extreme-UV lithography,[2,3] X-ray lithography,[4] and plasmonic lithography[5,6]); (b) charged particle-based lithography (electron-beam lithography[7,8] and focused-ion-beam milling[9]); (c) printing-based lithography (nanoimprinting[10] and micro-contact printing[11,12]); (d) direct laser writing;[13] (e) tip-based lithography (dip-pen lithography[14,15] and thermal tip lithography[16]); and (f) various self-assembly methods.[17,18] Photon-based lithography is currently widely used in industry, but the resolution is limited by the light diffraction effect. To further increase the resolution, both light sources with shorter wavelengths and the corresponding photo resists need to be developed. At the same time, lithography systems are getting more and more complicated with the decreasing feature size (*e.g.*, the use of an immersion type lithography system). Charge particle-based lithography (electron-beam, ion-beam) provides high resolution, but suffers from issues, such as a slow speed, low throughput, and complicated tool setup. Moreover, patterning can only be performed over a limited area due to the intrinsic low speed. In comparison, printing-based lithography is compatible with rich groups of materials and can be scaled to pattern structures over large areas. In addition, its throughput is high and many of the printing methods do not reply on complicated tool designs, making the fabrication highly efficient and inexpensive.

Nanoimprint lithography (NIL) is an important member of the printing-based lithography family. It was proposed in the 1990s by Chou and co-workers.[19,20] The technique involved a modification of the manufacturing process of compact disks and was also similar to a molding process developed by Japanese researchers in the 1970s.[21] In the nineties, nanoimprinting's demonstration of 10 nm feature sizes made it a promising alternative to the expensive UV optical lithography for the semiconductor industry. It is worth noting that this technique is not limited to patterning nano-scale features only; it can also fabricate structures of various dimensions, ranging from sub-10 nm to the micrometer or even millimeter scale. Thus, in the following discussions, "nanoimprinting" and "imprinting" are used interchangeably.

[a] Department of Electrical Engineering and Computer Science, University of Michigan, Ann Arbor, MI, 48105, USA. E-mail: guo@umich.edu
[b] Omega Optics, Inc., 8500 Shoal Creek Blvd, Building 4, Suite 200, Austin, TX, 78757, USA
[c] Microelectronics Research Center, Department of Electrical and Computer Engineering, University of Texas at Austin, Austin, TX, 78758, USA
† Current address: Department of Mechanical and Automotive Engineering, Seoul National University of Science and Technology, Seoul, 01811, Korea.

Published on 18 April 2016. Downloaded by University of Texas Libraries on 14/06/2016 15:37:27.

Although NIL has been in existence for over 20 years, several critical issues are still being identified and solved so that it can be employed in the highly demanding semiconductor industry. First, NIL is conducted with a 1× mask (typically called the imprinting mold/template). Therefore, in order to perform NIL, an expensive and high-precision mask needs to be prepared first. Also, NIL is a contact process, wherein defects can easily be generated and pattern distortions can happen during the mold/substrate separation (de-molding) process. Moreover, there is usually a residual layer left on the substrate after NIL, which needs to be removed before subsequent processing. However, the above constraints can be well tolerated by other applications, such as photonics, magnetics (*e.g.*, patterned media), sensors, micro-/nano-fluidics, and biology. Indeed, NIL's high resolution, great repeatability, low cost, and high-throughput ability make it an advantageous approach for both research prototype fabrication and future large-volume manufacturing for these applications.

In this review, NIL as well as its applications in photonic devices are discussed in detail. Its operational principle, processing methods, and materials will be explained, and various imprinted photonic elements will be surveyed. Imprinting has numerous advantages, including a simplified fabrication, high resolution, great fidelity, and increased throughput. Also, this method is capable of processing various kinds of materials on diverse substrates. All these unique features enable its application in high-performance printed photonic devices, including optical interconnects, photonic sensors, transparent conductors, and metamaterials. At the end of this article, other related techniques are also described, such as direct laser writing and dip-pen lithography, together with their applications in fabricating photonic elements.

2. Nanoimprinting: methods and materials

The originally proposed NIL used a hard mold to deform thermal plastic polymers through heating and applied pressure, creating a reverse replica of the mold pattern on the polymer layer.[19,20] Subsequently, UV-NIL was developed, where a UV-curable precursor was used as the resist material.[22,23] Compared with thermal-NIL, UV-NIL is performed at room temperature; also it has better overlay accuracies. Now, commercial NIL tools are available from various manufacturers, such as Nanonex, EVGroup, Obducat, Molecular Imprints, Eulitha, Sematech, and NIL Technology.

2.1 Mold preparation

Molds play a key role in the imprinting process. They can be made from hard materials, such as silicon (Si);[24] dielectrics, such as silicon oxide and silicon nitride;[25] metals, such as nickel;[26] soft materials, such as polydimethylsiloxane (PDMS)[27–30] and perfluoropolyether-based (PFPE) polymers;[31–33] and UV-curable resins.[34,35] Fig. 1a and b show the scanning electron micrographs (SEMs) of two Si hard molds (one-dimensional (1D) gratings and two-dimensional (2D) meshes), while Fig. 1c shows the picture of a large-area flexible PDMS mold. Compared to hard molds, soft molds are usually cheaper and provide better contact with the substrate, even when the substrate is curved or has irregular patterns. In addition, de-molding is usually easier for soft molds, especially in the case of large-area imprinting. However, the critical dimension achieved by a soft-mold is not as high as that of a hard mold, due to its low Young's modulus, and subsequent mold distortion during the imprinting process. Imprinting molds can be

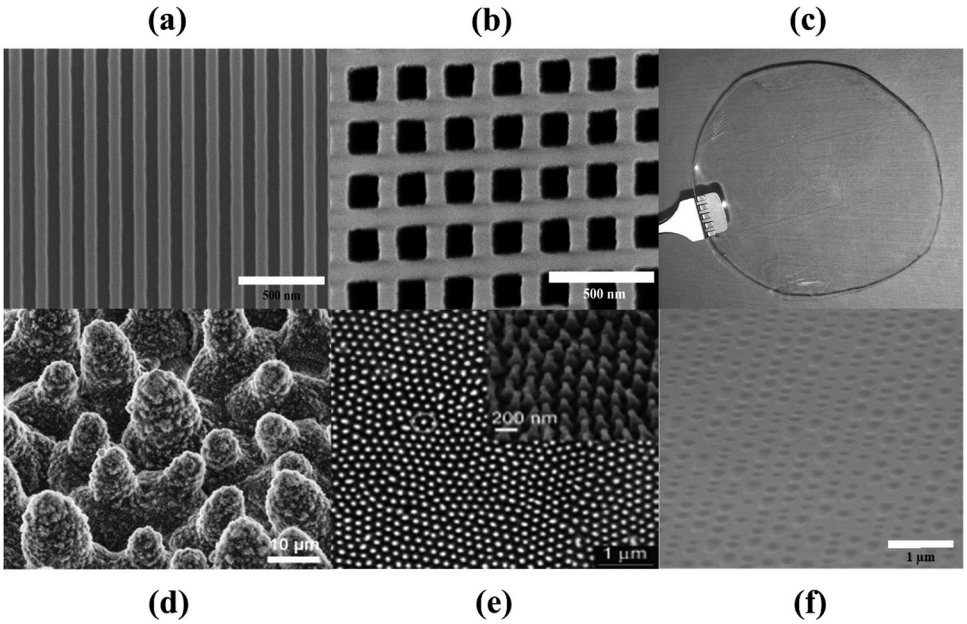

Fig. 1 Various imprint molds: (a) 1D grating mold on a Si substrate; (b) 2D mesh on a Si substrate; (c) a large-area, 4 inch PDMS flexible mold. (d) SEM picture of a lotus leaf. Reproduced with permission ref. 43. Copyright 2011, Beilstein Journal of Nanotechnology. (e) SEM picture of a cicada wing. Reproduced with permission ref. 41. Copyright 2006, John Wiley and Sons. (f) SEM picture of a Blu-ray movie disk. Reproduced with permission ref. 42. Copyright 2014, Nature Publishing Group.

 This journal is © The Royal Society of Chemistry 2016

Published on 18 April 2016. Downloaded by University of Texas Libraries on 14/06/2016 15:37:27.

fabricated by photolithography (for large-scale features) or electron-beam lithography (for small-scale features). Interference lithography has been employed to produce nano-scale patterns (such as 1D gratings) over a large area, and this method is usually faster and cheaper than electron-beam lithography.[36,37] Molds with complicated patterns can also be generated from molds with simple patterns, such as 1D gratings. For example, 2D pillars or meshes can be fabricated by performing imprinting twice with the 1D grating mold.[10,38] A new 1D grating mold with half the pitch of the original 1D mold can be generated using the method called "spatial frequency doubling".[39] Interestingly, some plants, animals, and our daily supplies also provide useful templates for making the imprint molds. For example, lotus leaves (SEM shown in Fig. 1d) and butterfly wings contain nano-scale features (*e.g.*, gratings, pillars, and meshes), and can be used to fabricate non-wetting (self-cleaning) surfaces.[40] Cicada wings (SEM shown in Fig. 1e) have periodic nanopillars arranged in a hexagonal fashion, and provide imprint molds to fabricate anti-reflection coatings.[41] Blu-ray movie disks (SEM shown in Fig. 1f) provide imprint templates for quasi-random nanostructures to enhance light trapping in solar cells.[42]

Since imprinting is a high fidelity process, imperfections (such as edge roughness) on the mold can be transferred onto the imprinted structures, resulting in a degrade in device performance. Several methods have been studied to mitigate this issue, including resist reflow, thermal oxidation, and laser liquefaction. Resist reflow is applied before using the resist as an etching mask to transfer the patterns onto the mold substrate. Here, the exposed and developed resist undergoes a thermal treatment, which helps to smooth out the resist line edge roughness induced by the lithography step.[44] Thermal oxidation is usually used to improve the quality of Si molds: the mold is kept in a high temperature furnace (filled with either air or oxygen), where the outside layer of the silicon is converted to thermal oxide (SiO_2), and this oxide layer is subsequently removed by a buffered hydrofluoric acid (BHF) etch (wet-etching). After this treatment, the Si mold sidewall roughness is significantly reduced.[45] Chou *et al.* proposed another method called 'self-perfection by liquefaction'.[46] In this process, a short laser pulse (duration of hundreds of nanoseconds) selectively melts the nanostructures (for example, gratings and pillars made of silicon or chromium), and at the same time, a set of boundary conditions (for example, one or more plates placed in contact with or in a gap above these structures) is applied to guide the flow of the molten materials into the desired geometries before their solidification, thereby significantly reducing the line edge roughness.

2.2 Imprinting procedures

After the molds are fabricated, they are coated with self-assembled fluoro-containing monolayers for surface energy reduction,[47] which facilitates the subsequent de-molding process. Imprinting can be generally categorized into thermal and ultraviolet (UV) imprinting, with the relevant schematics shown in Fig. 2a and b, respectively. In thermal imprinting, a layer of thermal plastic resist is mechanically deformed by the mold under pressure at an elevated temperature.[19,20] In practice, the temperature is set at about 70–90 °C above the polymer's glass transition temperature

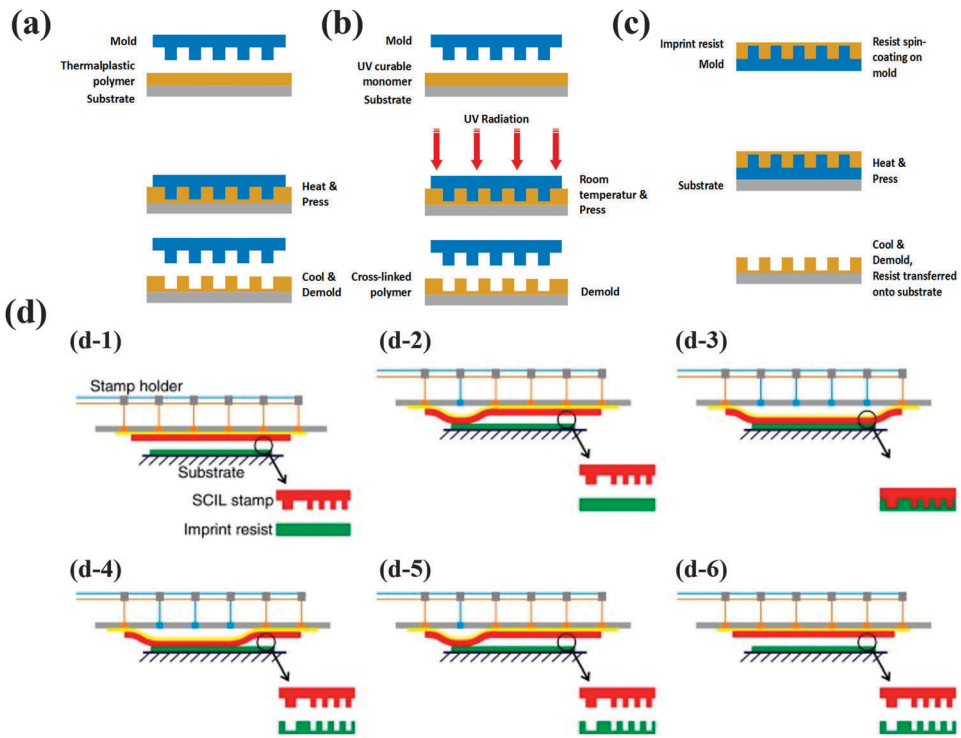

Fig. 2 Schematics of various imprinting methods: (a) thermal imprinting; (b) UV imprinting; (c) reverse imprinting; (d) substrate conformal imprinting. Reproduced with permission ref. 50. Copyright 2010, Elsevier.

Published on 18 April 2016. Downloaded by University of Texas Libraries on 14/06/2016 15:37:27.

(T_g) so that the polymer material reaches a viscous flow state.[48] For some applications where the resists are functional polymers, high temperatures can potentially cause polymer degradation. In addition, if the mold and substrate are made of different materials and have mismatched thermal expansion coefficients, high imprinting temperatures will also cause mold–substrate misalignments. The above issues can be mitigated by UV imprinting, wherein a layer of UV-curable monomer is deformed by the mold at room temperature and is simultaneously cross-linked by UV radiation.[22,23,49] Compared to thermal imprinting, UV imprinting has the advantages of a reduced imprinting pressure, room temperature operation, fast processing speed, and better alignment accuracy.

Substrate conformal imprint lithography (SCIL) is a recently developed imprinting method based on the principle of UV-NIL.[50] In SCIL, a flexible mold (usually made of PDMS) is mounted on a rigid glass carrier and kept in place by vacuum grooves. Imprinting is performed onto the substrate by the sequential release of each of the vacuum grooves between the PDMS mold and the glass carrier in a single direction. This results in minimized air inclusions, even over large areas. After the resist is cured, the mold is separated from the substrate by resealing the vacuum grooves in a reverse manner. The sequential separation of the stamp and substrate avoids excessive forces during imprinting and allows for a clean and reliable de-molding without inducing damage to the patterned structures (Fig. 2d). SCIL combines the advantages of large-area imprinting facilitated by soft molds and high resolution provided by rigid molds. This SCIL technique was developed by Philips Research (Eindhoven, the Netherlands) and SUSS MicroTec (Munich, Germany), and its toolkit can be installed on SUSS Mask Aligners.

When the substrate is not suitable for resist spin-coating or has a pre-defined surface topography, it is difficult to perform imprinting based on the previously described methods. Reverse nanoimprinting has consequently been developed to address these situations.[51,52] Here, instead of directly coating the resist on the substrate, it is spin-coated on the mold first and thus, a replica of the mold pattern is created in the resist layer. Afterwards, the patterned resist layer is transferred from the mold onto the substrate by performing imprinting (usually with a lower temperature and pressure than with normal nano-imprinting). The key to this successful transfer is that the mold has a lower surface energy than the substrate, and therefore, the resist layer has a better adhesion to the substrate. By performing multiple reverse imprintings, 3D nanostructures can be fabricated. Some metals, such as gold (Au) and silver (Ag), have weak adhesion with the Si surface. This property can be utilized to form Au or Ag nanostructures on Si surfaces first, and then these nanostructures can be transferred to other substrates by reverse printing.[53–55]

In general, the imprint mold consists of a combination of nano-scale and large-scale patterns. During imprinting, the large-scale features need to displace more imprint resist over longer distances than the nano-scale ones, and therefore, large-scale patterns are more difficult to be imprinted. Consequently, imprinting with molds with nano-scale patterns next to large-scale

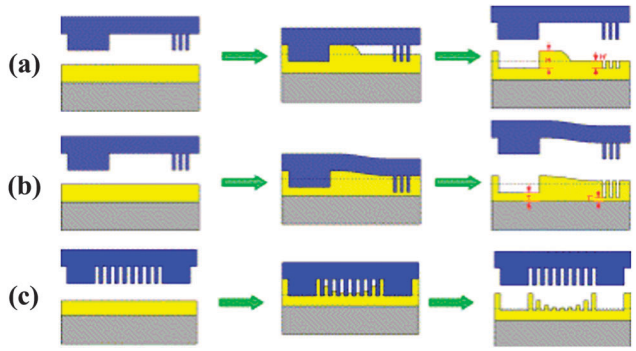

Fig. 3 (a) Non-uniform pattern height during NIL; (b) non-uniform residual layer thickness during NIL; (c) incomplete pattern transfer during NIL. Reproduced with permission ref. 56. Copyright 2004, Elsevier.

patterns can be challenging.[56] If a low pressure is used during imprinting, there will be no bending in either the mold or the substrate, and the patterns on the mold will penetrate into the resist layer on the substrate in a parallel fashion. Because of the viscous resist flow, it takes a much longer time (sometimes even impractically long in the timeframe of NIL) for the large-scale patterns to fully protrude into the resist layer and thus, this leads to an incomplete molding (Fig. 3a). In contrast, if a high pressure is applied instead, either the mold or the substrate will bend and there will then be conformal contact between them. As a result, nano-scale features penetrate deeper into the resist layer than the large-scale ones (non-uniform residual layer thickness), which can cause problems for the subsequent residual layer etching and pattern transfer (Fig. 3b). Similarly, molds with complex patterns will give rise to a random distribution of the recessed areas on the molds, and some patterns cannot be truthfully duplicated on the resist. For example, Fig. 3c shows a scenario where nano-scale patterns are next to large-scale patterns on the mold, and the imprinted structure has incompletely filled-in central parts. To avoid the above issues, one approach is to put some dummy features around the pattern areas in order to achieve the same "fill factor" over a large area. Researchers have also used NIL to define the nano-scale features first, and then used photolithography (with alignment) to subsequently define the large-scale features.

Another novel approach to fix the above limitation is the "combined-nanoimprint-and-photolithography (CNP)" technique (Fig. 4a). In CNP, the hybrid mold is made of UV transparent materials, and act as both a NIL and photolithography mask. Protrusions are made on the mold for imprinting nano-scale features, while metal pads are fabricated on the mold as a mask for photolithography. The mold is first imprinted into the resist, which can be either a UV-curable monomer or negative tone photoresist, and then the whole mold–substrate assembly is exposed to UV radiation. After de-molding, the substrate is immersed in a developer solution to remove the un-exposed area. As a result, both the nano-scale and large-scale features on the mold can be faithfully transferred onto the substrate. The CNP approach can also be applied to create imprinted structures free of residual layers (Fig. 4b).[57] Molds with thin

 This journal is © The Royal Society of Chemistry 2016

Published on 18 April 2016. Downloaded by University of Texas Libraries on 14/06/2016 15:37:27.

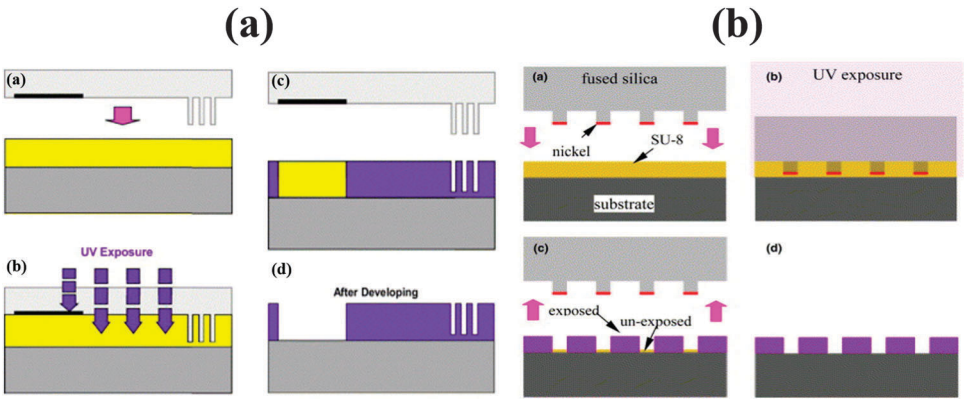

Fig. 4 (a) Schematic of CNP using a hybrid mold to fabricate both nano-scale and large-scale features simultaneously. Reproduced with permission ref. 56. Copyright 2004, Elsevier. (b) Schematic of CNP using a mold with light-blocking layers on top of the protruding patterns to fabricate residual-layer-free imprinted structures. Reproduced with permission ref. 57. Copyright 2004, Elsevier.

metal layers on top of the protruding patterns are prepared first. During imprinting, the area underneath the protruding nanostructures are not exposed, and therefore, they are fully removed by the developer after de-molding.

Imprinting can also be carried out directly on substrates without using any resist. Buzzi *et al.* proposed using Si molds to pattern metal films (such as Ag and Au) at a high temperature (400 °C) and pressure (300 MPa), with the Si molds subsequently removed by wet-etching.[58,59] This method can be thought of as a micro-scale metal embossing/forging, and is effectively the same technique used to make coins. Varghese *et al.* improved the above method and demonstrated a low pressure (<4 MPa) and temperature (25–150 °C) imprinting of Ag and Au plasmonic nanostructures with Si molds, which could be recycled multiple times.[60] Here, although the applied imprinting pressure is low, the contact area between the mold and metal film is so small that the local pressure is orders of magnitude higher. When the pressure is higher than the metal's yield strength, the plastic flow of the metal film allows the mold to protrude into it. Chou and Cui *et al.* proposed "laser assisted direct imprinting", where an excimer laser is first used to melt the surface of Si or metal films, and then a quartz mold (which is transparent to the excimer laser light) is pressured onto the substrate.[61,62] The demonstrated resolution was better than 10 nm and the embossing time was as short as hundreds of nanoseconds.

To attain faster processing speed, roll-to-roll imprinting has been gaining increased attention. Fig. 5 demonstrates a scalable fabrication process of small-scale structures through continuous roll-based nano-patterning techniques. Fig. 5a depicts the roll-to-roll (R2R) imprinting of subwavelength-scale dot patterns on a metal–insulator–metal (MIM) stacked polymer film using a flexible stamp with the inverse profiles.[63,64] As the rolling proceeds under conformal contact between the stamp roll and the substrate roll, the stamp continuously imprints the patterns on a linearly-fed substrate typically coated with UV-curable resins, which are subsequently cured by UV light at the outlet of the contact zone. Not only can the R2R principle be utilized in a continuous nanoimprinting, it can also be adopted to scale up the traditional contact-based photolithography. Photo roll lithography (PRL)[65] is one such example. Fig. 5b illustrates its process schematics: a flexible photomask is attached to a hollow quartz roll within which a downward-collimated UV light is mounted. A photoresist-coated substrate is then fed underneath the roll, under conformal contact or in proximity, and is continuously illuminated by the UV light. The patterning step is completed by feeding the substrate through

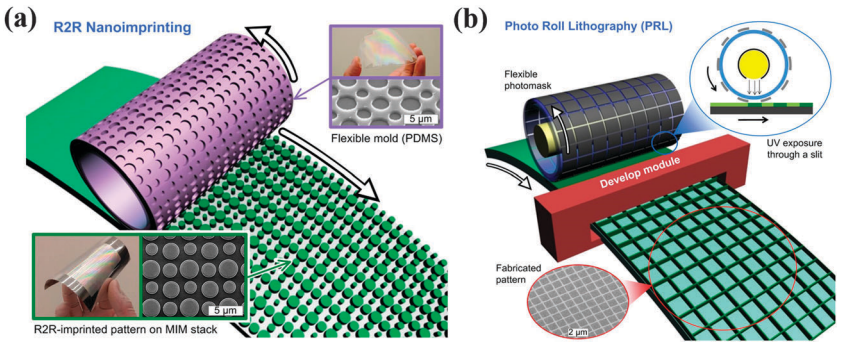

Fig. 5 (a) Schematic of roll-to-roll (R2R) nanoimprinting for the continuous fabrication of plasmonic dot patterns on a metal–insulator–metal (MIM) stack. Reproduced from ref. 64. Copyright 2012, the American Institute of Physics. (b) Schematic of the photo roll lithography (PRL) processing of Al metal mesh patterns on PET film. Reproduced from ref. 65. Copyright 2013, John Wiley and Sons.

Published on 18 April 2016. Downloaded by University of Texas Libraries on 14/06/2016 15:37:27.

the developing module. By controlling the relative motion between the mask and substrate, identical or elongated patterns can be produced. A variety of thin-layered, geometrically-tunable photonic structures can therefore be fabricated by R2RNIL and PRL in a continuous and scalable fashion, including wire-grid polarizers,[66] color filters,[67] solar cells,[68,69] flexible electronic devices,[70,71] and optical filters.[64,65]

In addition to the aforementioned roll-based methods, a series of other methodologies have also been inspired by continuous and dynamic printing principles (*i.e.*, pullout, pressing, indenting, and forging), as shown in Fig. 6. Dynamic nano-inscribing (DNI)[72] realizes a continuous creation of seamless grating structures over substrates of any length, by sliding the cleaved grating mold edge over a compliant polymer substrate under conformal pressure and proper heating (Fig. 6a). DNI can be applied to many polymer films, and the resulting pattern profiles can be controlled by the localized heating. The nature of the conformal line (*i.e.*, the tool edge) in the contact-based patterning of DNI enables continuous patterning on flat or curved surfaces, as well as along circular or bent paths (Fig. 6c).[72] Another technique, vibrational indentation-driven patterning (VIP) (Fig. 6b),[73] can achieve the real-time pitch-tunable fabrication of grating structures on various polymer

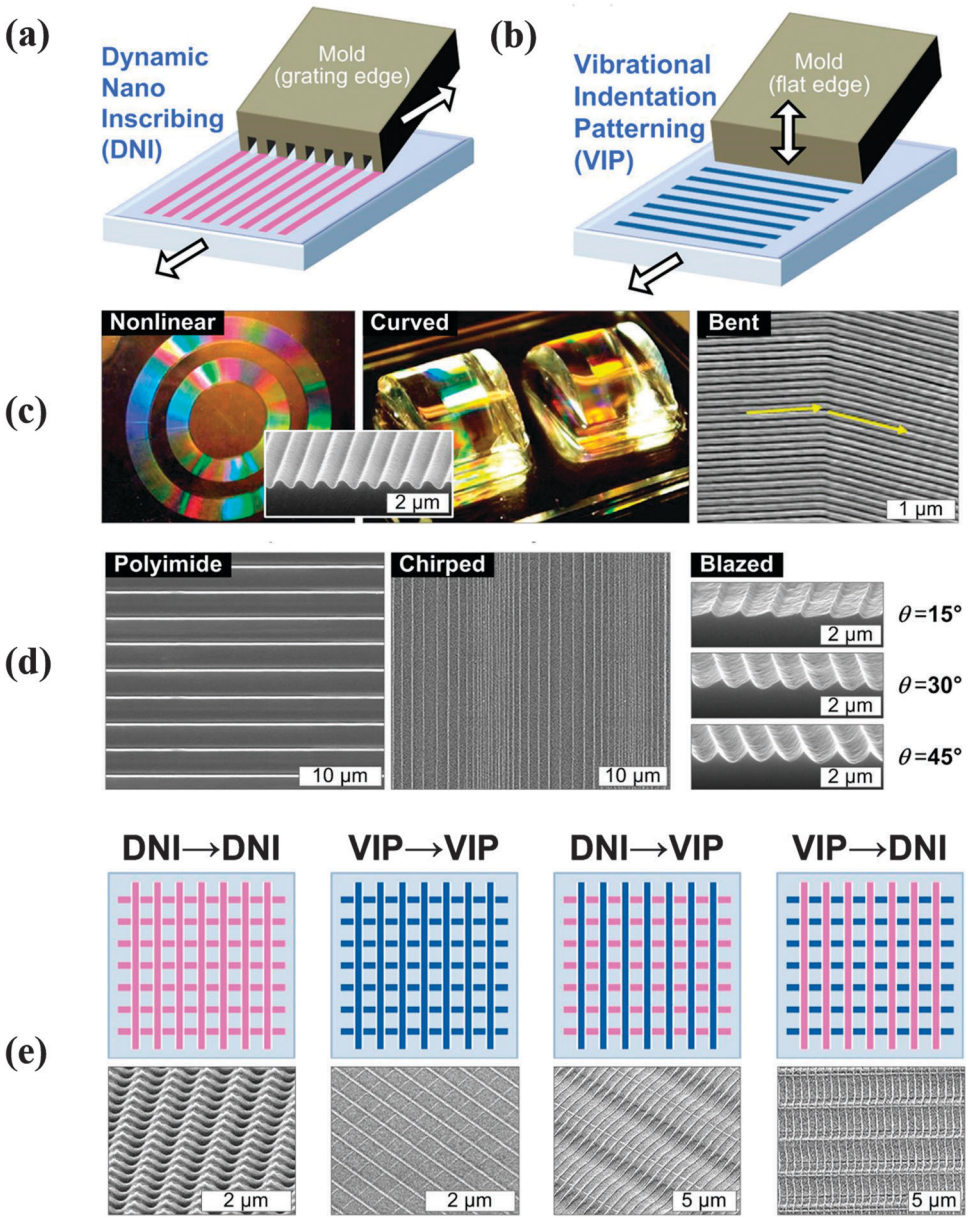

Fig. 6 Schematic of (a) dynamic nano-inscribing (DNI) and (b) vibrational indentation patterning (VIP) processes. Reproduced from ref. 74. Copyright 2014, Royal Society of Chemistry. (c) Various patterning examples fabricated by DNI. Reproduced from ref. 72. Copyright 2009, American Chemical Society. (d) Various patterning examples fabricated by VIP. Reproduced from ref. 73. Copyright 2013, John Wiley and Sons. (e) Multidimensional nano-patterning schemes and representative SEM images, enabled by the combination of DNI and VIP. Reproduced from ref. 74. Copyright 2014, Royal Society of Chemistry.

 This journal is © The Royal Society of Chemistry 2016

Published on 18 April 2016. Downloaded by University of Texas Libraries on 14/06/2016 15:37:27.

materials. It utilizes the high-frequency vertical vibration of a rigid flat edge to periodically create indentations of line patterns on a horizontally-moving substrate. By adjusting the tool angle, vibration frequency, and the substrate moving speed, diverse grating patterns, such as pitch-variable chirped gratings, and angle-variable blazed gratings, can be created in a continuous and high-throughput manner (Fig. 6d). Moreover, DNI and VIP can be combined to fabricate various 2D and multidimensional micro- and nano-scale patterns, as demonstrated in Fig. 6e.[74] Many photonic applications, especially those that require nonlinear, tunable, and multidimensional pattern architectures, may benefit from such processes.

2.3 Imprint resists

After imprinting is completed, the patterned resist can be subsequently employed as a mask to transfer the patterns to the substrate beneath (by etching or lift-off), or the resist itself can directly function as part of the photonic devices. Compared to other lithography techniques, nanoimprinting is capable of processing a variety of materials. Table 1 lists some commonly used imprint resists and their processing conditions. High-refractive-index materials (refractive index of around 2 or even higher) are promising for building compact micro- and nano-scale photonic devices and light circuitry. However, such a high refractive index is not easily attainable in organic materials. Toward this end, titania-based NIL resists using sol–gel chemistry have been developed.[75,76] Lastly, the properties of imprinting resists can be further enriched by doping them with functional groups, such as quantum dots and organic dyes.[77–79]

3. Imprinted photonic elements

3.1 Optical interconnects

Traditional electronic interconnects have constraints, such as a limited operating speed, electromagnetic interference, and power and heat dissipation issues at high operating frequencies.[93,94] Optical interconnects not only can address the above issues, but also provide additional benefits, such as wavelength-division multiplexing capabilities and a reduced power consumption.[95,96] Polymer-based photonic devices are attractive candidates for low-cost and high-performance optical interconnects due to their compatibility with Si and GaAs fabrication technologies,[97,98] and ability to be integrated with various passive and active devices.[99] In addition, the refractive index of most polymers (1.5–1.7) is nearly matched to that of glass optical fibers (1.5–1.6), resulting in only a small Fresnel reflection loss at the interfaces in the butt-coupling of waveguides and input/output fibers. Also, single mode polymer waveguides have lower index contrast and thus provide better mode-matching with single mode fibers compared to silicon waveguides. Moreover, there are a range of low-loss optical polymers in the telecommunication band, such as poly(methyl methacrylate) (PMMA), SU8, polystyrene (PS), organically modified ceramics (ORMOCERs), *etc.*, and their absorption loss can be below 0.1 dB cm^{-1}.[100] At last, polymers are spin-on films so they can be easily spin-coated onto various substrates, which simplifies the fabrication.

One common method to fabricate polymer-based optical interconnects is to use lithography techniques (*e.g.*, photo lithography) to define patterns into the resist first, and then to transfer the patterns from the resist to the optical polymer *via* plasma etching.[101,102] This method is straightforward, but not cost-effective due to the complicated fabrication process and low throughput. Another approach is to directly pattern a low-loss UV-curable polymer by lithography. However, this method has limitations of poor dimension and profile control (*e.g.*, results in a rough surface morphology of the patterned resist) due to the effects of wave diffraction, as well as interface and substrate scattering in the lithography step. In addition, UV photo bleaching is another method to form a photonic waveguide by creating a refractive index variation of the polymer core in the passive regions of the waveguide; however, the polymer

Table 1 Commonly used imprint resists and their processing conditions

Name	Imprinting condition	Notes
Poly(methyl methacrylate) PMMA	Thermal (140–180 °C, 600–1900 PSI[80])	One of earliest imprint resists, and also a popular positive tone Ebeam resist
Polystyrene (PS)	Thermal (180 °C, 600 PSI[81,82])	Has been used to make waveguide devices, such as a microring resonator
Polycarbonate (PC)	Thermal (220 °C, 1066 PSI[82])	Tough polymer material that can endure the de-molding forces after NIL
NEB22	Thermal (120–140 °C, 725 PSI[83])	Formulated by SUMITOMO chemical, and also works as a negative tone Ebeam resist
PVPK	Thermal (90 °C, 101 PSI[84])	Better etching resistance than PMMA
Cyclic olefin copolymer (COC)	Thermal (170 °C[85])	Highly transparent, chemically resistant, and low water absorption
MR series	Thermal, UV or combined thermal and UV	Commercial imprint resists from Micro Resist Technology Inc.
SU8	Combined thermal and UV[56,86]	Commonly used negative tone photo resist
Cytop	Thermal (150 °C, 600 PSI[87])	Formulated by ASAHI Glass. Low surface energy. Used for fabricating imprint molds[88] or nanofluidic channels[87]
UV15 series	UV[89]	Commercial product from Masterbond Inc.
Ormostamp	UV[90]	Commercial imprint resists from Micro Resist Technology Inc. Used for imprint mold duplication
Ormocore/clad	UV[91]	Commercial imprint resists from Micro Resist Technology Inc.
NOA series	UV[92]	Commercial UV-curable resins from Norland Inc.

Published on 18 April 2016. Downloaded by University of Texas Libraries on 14/06/2016 15:37:27.

material has to be electro-optically (EO) active, which limits this method's wider application.[103,104] Instead, imprinting can effectively overcome the above shortcomings. Imprint molds can be carefully prepared to have smooth profiles (such as by resist reflow or thermal oxidation, as discussed in Section 2.1), and therefore, the imprinted structures can have significantly improved profiles compared to their counterparts fabricated by plasma etching or direct photon/electron exposure.[45,105] Moreover, imprinting is compatible with various thermal or UV-curable materials (details discussed in Section 2.3), and at the same time, provides roll-to-roll (R2R) patterning capabilities at both the micro- and nano-scale. Therefore, imprinting provides a viable solution for the high-rate manufacturing of low-cost polymer-based optical interconnects.

Various polymer-based optical interconnects have been demonstrated, including both passive and active devices. Passive devices include waveguides, splitters, combiners, interferometers, directional couplers, resonators, tapers, filters, and mode converters.[75,106–113] Multiple-layer interconnects can also be fabricated through aligned multiple steps of imprinting.[91] By employing polymers whose properties can be modulated by external stimuli (*e.g.*, by heating, electrical current, *etc.*), active optical interconnects, such as modulators and switches,[89,114–116] can be implemented. Here, a printed electro-optic (EO) modulator will be discussed as an example. EO modulators are capable of encoding electric signals onto optical carriers, and have various applications in high-speed communication networks, radar systems, high-frequency optical chopping, RF wave sensing, *etc.*[117–119] They can be made of different configurations, such as microring resonators,[120] Mach–Zehnder interferometers (MZIs),[89,121] directional couplers,[102] *etc.* A schematic of an EO modulator based on a Mach–Zehnder interferometer is shown in Fig. 7a. A voltage applied on the modulating arm causes a change in the refractive index of the constituent EO polymer, leading to a propagation phase change when light travels through this arm. Such a phase modulation ultimately translates to an intensity modulation at the output port of the MZI.

To fabricate such a device, a transparent mold made of epoxy silsesquioxane (SSQ)[198] was duplicated from a silicon hard mold first. Then, the transparent flexible mold was used to imprint the core region in a UV-curable resin (UV15LV), serving as a bottom cladding layer coated on a substrate with pre-defined Ag bottom electrodes. Afterwards, a layer of EO polymer (AJ-CKL1) was spun on the printed bottom cladding, which not only filled the imprinted core trenches, but also formed a planar top surface for the subsequent processing. Next, the top cladding layer made of UFC-170A was spun-coated and cured by UV radiation. Finally, the top silver electrodes were patterned using ink-jet printing, which concluded the device fabrication. Fig. 7b shows a cross-sectional SEM of the fabricated EO modulator. Note that the spin-coating method can easily be replaced with the ink-jet printing method for creating an 'all-printed' device platform.

To achieve EO activity, the EO polymer is poled first, wherein an electrical field (about 80 V μm^{-1}) is applied between the top and the bottom Ag electrodes. The temperature is increased from room temperature to the glass transition temperature of the EO polymer ($\sim$140 °C), and then quickly decreased to room temperature. For measuring the fabricated structure, a TM-polarized light at 1550 nm wavelength is launched into the

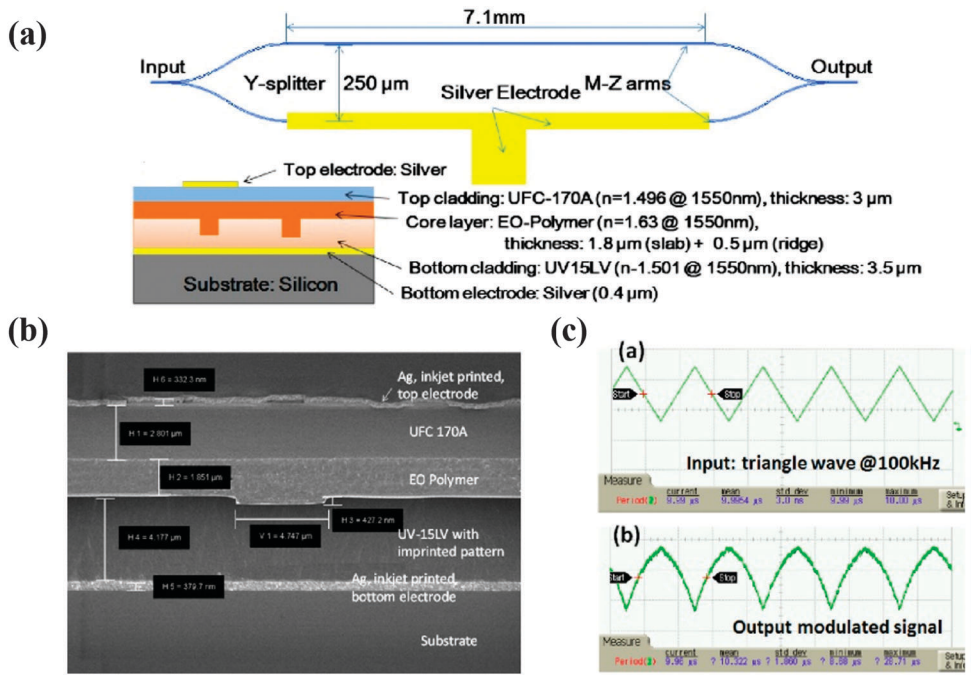

Fig. 7 (a) Schematic of a printed EO modulator. (b) Cross-sectional SEM of the fabricated EO modulator. (c) 100 KHz triangular electrical driving signal, and the corresponding modulated optical output signal from the EO modulator. Reproduced with permission ref. 89. Copyright 2013, Optical Society of America.

 This journal is © The Royal Society of Chemistry 2016

Published on 18 April 2016. Downloaded by University of Texas Libraries on 14/06/2016 15:37:27.

device using a single mode lensed fiber, and the output light is collected by another lensed fiber. Fig. 7c shows the modulated output signal when a 100 KHz triangular wave is applied across the electrodes.

3.2 Optical sensors

Optical sensors have many advantages over conventional electronic sensors, such as high sensitivity, compact size, multiplexing capability, and robustness against electromagnetic interference. On-chip optical sensors have various forms, such as photonic crystals,[122–124] plasmonics,[125,126] metamaterials,[127,128] and microresonators.[129–131] Their sensing mechanism can be generally understood to be due to the devices' optical characteristics (*e.g.*, transmission, reflection or absorption) being affected by external stimuli, which may be biochemical/gas molecules,[132–134] mechanical vibrations,[135,136] temperature variations,[137] electromagnetic waves,[101,119,138] *etc.* Low-cost and large-scale sensors that can be manufactured at high volumes are in demand. Fortunately, these requirements can be easily met by the simplified fabrication, increased throughput, and improved reproducibility of NIL.[10] As an example, a printed optical microring resonator as well as its applications in refractometric sensing and acoustic wave detection are discussed below.

Fig. 8a shows the schematic of a microring resonator. The device consists of a straight waveguide and a circular waveguide in close proximity.[139] A microring with this configuration can be treated as a miniature Gires–Tournoise etalon (reflection type Fabry–Perot interferometer), wherein one end of the bus waveguide serves as the input and the other end as the output. Light is coupled in and out of the ring in the small gap region between the ring and the straight waveguide. At certain input wavelengths, there are constructive interferences inside the ring, leading to transmission intensity dips at the output.[105] The resonant wavelengths are determined by various factors, including the ring diameter, the cross-section area, and the refractive indices of both the ring itself and its surrounding media. Any perturbation of the above factors will lead to resonant wavelength shifts of the device, which is the foundation of optical sensing with microring resonators.

Two sensing schemes can be utilized by looking at the device transmission behavior: monitoring the resonant wavelength shift with input light of tunable wavelengths (Fig. 8d), or monitoring the output intensity variation with input light of a fixed wavelength (Fig. 8e). The former scheme provides a wider detection range, but requires a complicated setup for the spectrum measurements. For the latter scheme, the input laser wavelength is fixed at the slope of the ring resonance curve, and therefore, a tiny shift of the resonant wavelength will be converted to a varied output intensity. However, this method is limited to a narrow detection region, which is about half of the resonant bandwidth or even narrower. For both schemes, the detection sensitivity is closely related to the device's quality factor (Q factor), defined as $\frac{\lambda}{\Delta\lambda}$, where λ is the resonant wavelength and $\Delta\lambda$ is the full width half maximum (FWHM) of the resonance curve. A high Q factor denotes a sharp resonance curve, and thus, a higher detection sensitivity.

There are various ways to fabricate polymer microrings, including using electron-beam lithography, photolithography, or imprinting to directly pattern the polymers, or by first using the above techniques to define features on different materials and then subsequently transferring the patterns onto the polymers by etching. Compared with other methods, imprinting can pattern features of various dimensions in high fidelity and with great repeatability. By carefully optimizing the mold fabrication process (as explained in Section 2.1, particularly with thermal reflow and thermal oxidation), Si molds with smooth sidewall profiles can be obtained.[44,45] High quality molds contribute to printed polystyrene microrings with Q-factors in the order of 10^5 (Fig. 8b and c).[140] Moreover, imprinting could be expanded to roll-to-roll configurations for high-volume productions.

Biochemical sensing utilizes the evanescent wave outside the ring resonator to probe analytes on the sensor surface or in its surrounding medium. The presence of analytes modifies the

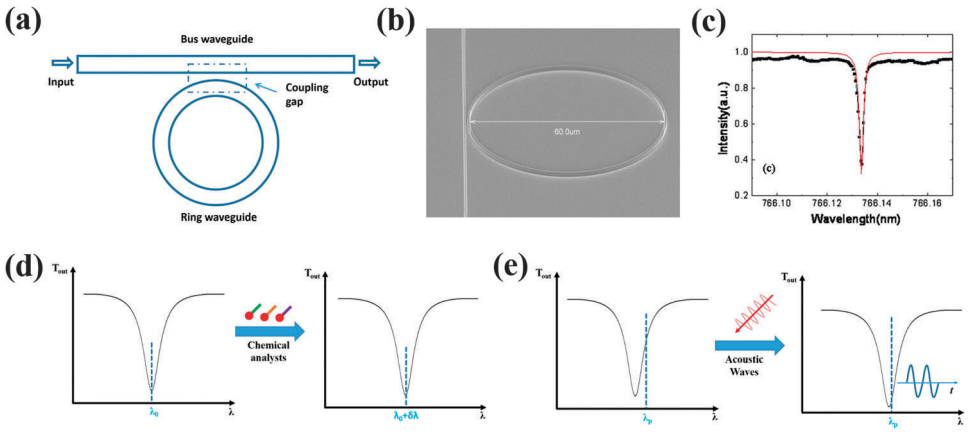

Fig. 8 (a) Schematic of a microring resonator. (b) SEM picture of an imprinted polystyrene (PS) microring resonator. Reproduced with permission ref. 81. Copyright 2014, American Chemical Society. (c) Transmission spectrum of a microring around 780 nm with a Q factor of 4×10^5. Reproduced with permission from ref. 140. Copyright 2011, AIP Publishing LLC. (d) Schematics of sensing by monitoring the resonant wavelength shift with input light of tunable wavelengths. (e) Schematics of sensing by monitoring the intensity variation with input light of a fixed wavelength.

Published on 18 April 2016. Downloaded by University of Texas Libraries on 14/06/2016 15:37:27.

effective refractive index experienced by the optical mode propagating inside the ring, thus changing the device's resonant wavelengths.[132] Polymers as constituent materials have the advantages of rich surface functionality as well as low cost and simple processing.[82] As mentioned earlier, the sensing can be implemented by either monitoring the resonant wavelength shift or by monitoring the output intensity change for a fixed laser wavelength. Based on the latter scheme, an imprinted polystyrene (PS) microring acts as a high-performance acoustic sensor. In this application, the incident ultrasound waves modulate the polymer refractive index (by the elastic-optic effect[141]), as well as deform the ring waveguide geometry, both of which change the device resonant wavelengths. If the probe laser wavelength is fixed at the sharp slope of the resonance curve, the ultrasound waves will be faithfully recorded using the time-varying output intensity from the microring output. The device has a flat frequency response from nearly DC up to ~350 MHz at −3 dB, as well as a low noise equivalent pressure (NEP) of 105 Pa over this band. Such a broad bandwidth leads to a record-high sub-3 μm axial resolution in photoacoustic imaging.[81] Microrings have been applied in various photoacoustic imaging systems, such as microscopy[142,143] and tomography,[135] as well as in non-imaging systems, such as real-time terahertz (THz) detection.[138,144]

3.3 Solar cells

Solar cells convert sunlight into clean electrical power, and provide a virtually unlimited supply of energy. To boost their power conversion efficiencies, one commonly used strategy is light management: *i.e.*, optimizing light absorption efficiency in the photoactive layer. This is especially important for thin-film based solar cells (*e.g.*, organic solar cells, thin silicon cells, *etc.*),[145,146] which have much thinner light absorption layers than their wafer-based crystalline counterparts. Various nanostructures have been proposed for light management in solar cells, for which Brongersma *et al.* provided an efficient and incisive summary.[147] NIL is a powerful tool to fabricate these nanostructures in a cost-effective and scalable fashion. One commonly used type of these approaches is textured substrates, which can scatter/diffract the incident sunlight and thus, increase its optical path in the absorbing layers. UV-NIL has been employed to transfer the nanostructures from a self-textured ZnO film into a UV-curable resin coated on glass substrates, and thin Si solar cells built upon such substrates have shown enhanced power conversion efficiencies (Fig. 9a).[148] Besides the advantages of repeated use of ZnO nano-textured molds, this imprinting method also avoids high temperature operation and is applicable in building solar cells on inexpensive, flexible polymer substrates (*e.g.*, PET).[149] To further reduce the cost of nano-textured molds, Blu-ray movie disks have been investigated as imprint templates. Interestingly, their quasi-random nanostructures, which were designed for optimizing data compression and error tolerance, are also nearly optimized for photo management in solar cells as well.[42] Besides the scattering effect, optical resonance has also been explored to enhance solar cell performance. For example, 1D silver (Ag) nanowires fabricated by NIL have been applied as semi-transparent anodes in organic solar cells (Fig. 9b).[150] When properly designed, the Ag nanowires can effectively couple the incident light to surface plasmon (SP) waves, which are enhanced electromagnetic fields at the interface between the metal and dielectric layers. Since the thickness of semiconductor layers in organic solar cells is typically tens of nanometers and is within the decay length of the surface plasmon resonance (SPR), SPR enhancement will boost light absorption in the photoactive layer and thus, enhance the power conversion efficiency (Fig. 9c). Parallel to light management, which promotes device performance from the "optical" perspective, there are also efforts to optimize the photoactive layer morphology in order to increase the exciton dissociation rates, as well as to facilitate charge carrier transport.[151,152] A vertically bi-continuous and inter-digitized

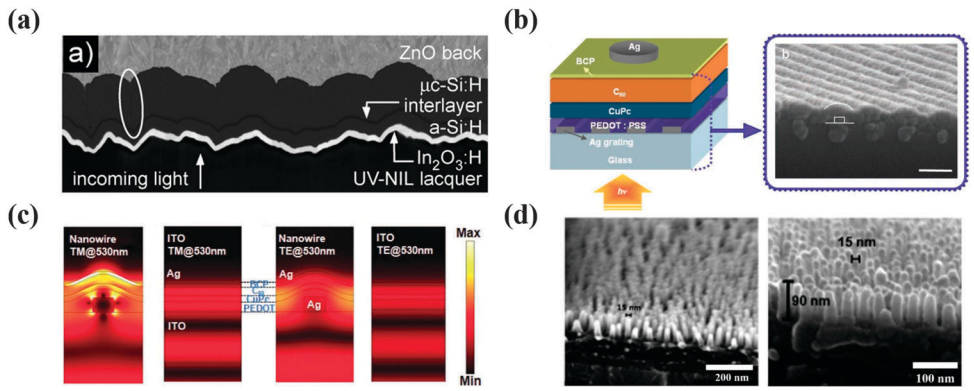

Fig. 9 Various imprinted structures in solar cells: (a) cross-section view of a Si solar cell with an imprinted textured substrate. Reproduced with permission ref. 148. Copyright 2010, American Chemical Society. (b) Schematic and SEM cross-section of a small molecular weight organic solar cell with a nanoimprinted Ag nanowire anode. (c) Simulated electric field profiles of Ag nanowire and ITO devices for TM- and TE-polarized incident light at the wavelength of 530 nm. There is enhanced light field in the active layer for the Ag nanowire solar cells. Reproduced with permission ref. 150. Copyright 2010, John Wiley and Sons. (d) High aspect ratio 15 nm scale imprinted organic semiconductor nanopillars: poly[*N*-9″-hepta-decanyl-2,7-carbazole-*alt*-5,5-(4′,7′-di-2-thienyl-2′,1′,3′-benzothiadiazole)] (PCDTBT), and a small molecular organic semiconductor fullerene derivative. Reproduced with permission ref. 153. Copyright 2015, John Wiley and Sons.

 This journal is © The Royal Society of Chemistry 2016

Published on 18 April 2016. Downloaded by University of Texas Libraries on 14/06/2016 15:37:27.

heterojunction between donor and acceptor has been regarded as one of the ideal structures for efficient charge separation and transport, and such structures can be fabricated by thermal NIL. This process could be further extended to solution-based soft-printing lithography, and in line with this, high aspect ratio polymer semiconductor nanopillars with a diameter of 15 nm were successfully demonstrated by utilizing a PDMS nanohole-type soft stamp (Fig. 9d).[153] Finally, to move toward the scalable fabrication of nanostructures over large areas, R2R NIL and SCIL have been employed.[154]

3.4 Plasmonic devices and metamaterials

Plasmonic devices and metamaterials, *i.e.*, electromagnetic structures engineered on subwavelength scales, exhibit extraordinary optical properties not offered by natural optical materials. The study of these devices has been a thriving research area over the past decade, and they have demonstrated numerous phenomena, such as extraordinary light transmission,[155] super-resolution imaging,[156] negative refraction,[157] cloaking,[158–160] hyperbolic dispersion,[161] anomalous refraction,[162] structural colors,[163,164] asymmetric light transmission,[165,166] and optical modulations.[167–169] To fabricate the constituent nanostructures (especially for devices working in the visible or NIR), both top-down (Ebeam, FIB, and NIL) and bottom-up approaches (various self-assembly methods) have been employed. Compared to other techniques, NIL provides an efficient and cost-effective way to fabricate plasmonic and meta-devices over large areas on various substrates. For example, large-area 1D grating molds manufactured by inexpensive interference photolithography can be employed to fabricate various meta-devices whose building blocks (unit cells) are in the "1D line" form, such as structural color filters (Fig. 10a)[163,170] and hyperbolic metamaterial absorbers (Fig. 10b).[171] Moreover, through performing imprinting twice with two 1D grating molds (or the same 1D mold) and by controlling the orientation between them, 2D plasmonic arrays of varied sizes, shapes and spacings were created (Fig. 10c).[172] For more complex patterns, the molds are usually first fabricated by other nanolithography techniques (*e.g.*, Ebeam, FIB, *etc.*). Compared to directly using Ebeam or FIB

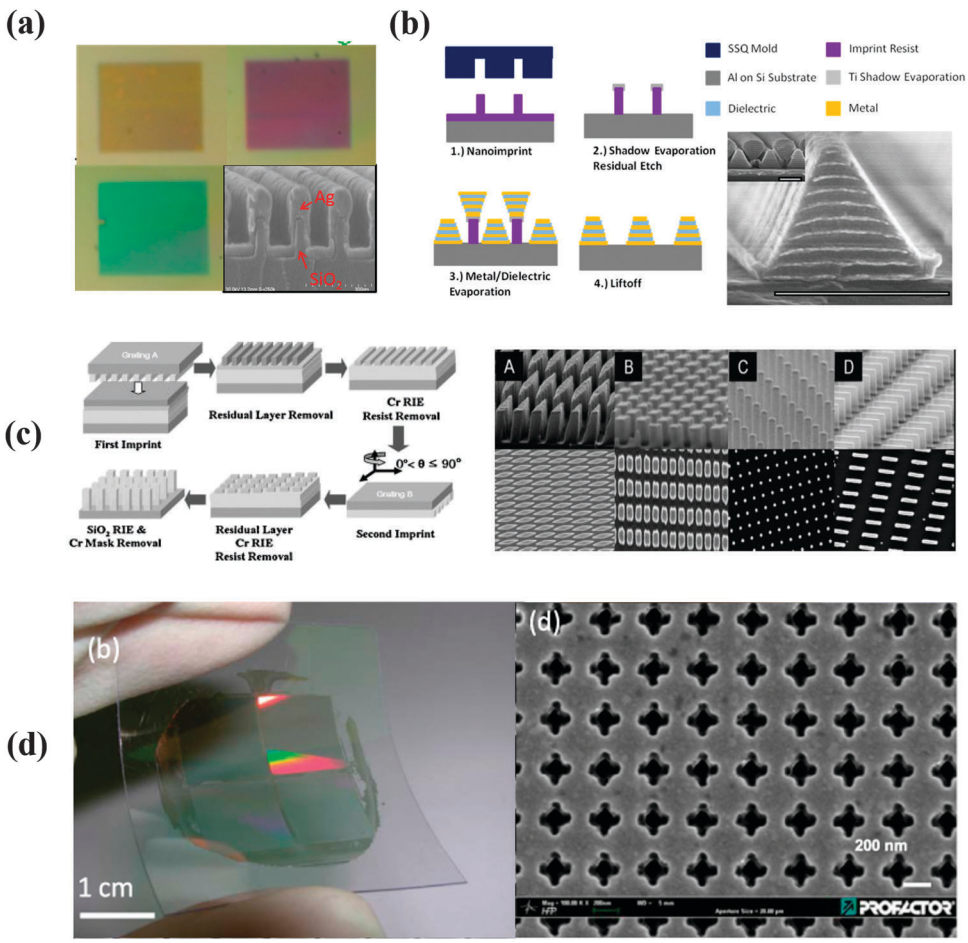

Fig. 10 Various imprinted plasmonic and metamaterials: (a) imprinted structural color filters with a corresponding SEM picture in the bottom right corner. Reproduced with permission ref. 163. Copyright 2013, Nature Publishing Group. (b) Left: Schematic of fabricating tapered hyperbolic metamaterials through NIL and metal/dielectric deposition and lift-off; right: SEM of the fabricated structure. Reproduced with permission ref. 171. Copyright 2014, American Chemical Society. (c) Left: Schematic of fabricating a 2D imprinting mold through imprinting twice with 1D molds; right: SEM of various imprinted plasmonic arrays. Reproduced with permission ref. 172. Copyright 2008, John Wiley and Sons. (d) Left: Printed negative index metamaterials (NIMs) on a flexible foil; right: SEM of the Swiss-cross NIMs. Reproduced with permission ref. 173. Copyright 2011, IOP Publishing Ltd.

Published on 18 April 2016. Downloaded by University of Texas Libraries on 14/06/2016 15:37:27.

to fabricate the devices, imprinting can significantly improve the throughput and can produce large-area samples with a high level of reproducibility. Based upon this approach, printed negative refractive index materials (Fig. 10d),[173–175] meta-absorbers,[176,177] and polarization conversion devices[178,179] have been demonstrated.

4. Beyond imprinting

4.1 Direct laser writing

Three-dimensional (3D) printing has attracted tremendous interest in recent years and is indispensable for rapid prototyping in applications ranging from industrial parts to everyday merchandize. However, the widely known 3D printing techniques usually cannot achieve resolutions down to the nano- or even micro-scale levels. Fortunately, direct laser writing (DLW) has the ability of 3D micro-scale printing (μ-printing), which is based on the nonlinear optical absorption and polymerization of photosensitive materials. Hohmann *et al.*, Fischer *et al.*, and Sugioka *et al.* provide comprehensive summaries of this technology.[180–182] The originally proposed DLW technique uses a NIR femto-second (fs) laser incident on the backside of the substrates (schematics shown in Fig. 11b, left part).[183] The laser is focused by an objective lens into the photosensitive materials (resins) coated on the front side of the substrate. Both the substrate and resins are transparent to the fs laser, which guarantees minimal attenuation of the incident fs laser. However, there is a strong optical field at the focus of the laser beam, and therefore, two-photon (or even multi-photon) absorption occurs inside this area, which consequently cross-links and solidifies the resins. By scanning the laser beam with a motorized 3D stage, complex 3D patterns are created. The achievable height of the written structure is limited by the working distance of the objective lens system. To further extend the printing range along the vertical direction, dip-in DLW has been developed.[184] Instead of shining the laser through the backside of the substrate, the laser is incident directly toward the front side, and the photosensitive resin serves as both the immersion media (refractive index matched with the substrates) and the photoresists (Fig. 11b, right part). Based on this geometry, structural heights up to several millimeters have been demonstrated.[184,185] To further increase the writing speed, galvanometric-mirror-based scanners have been developed,

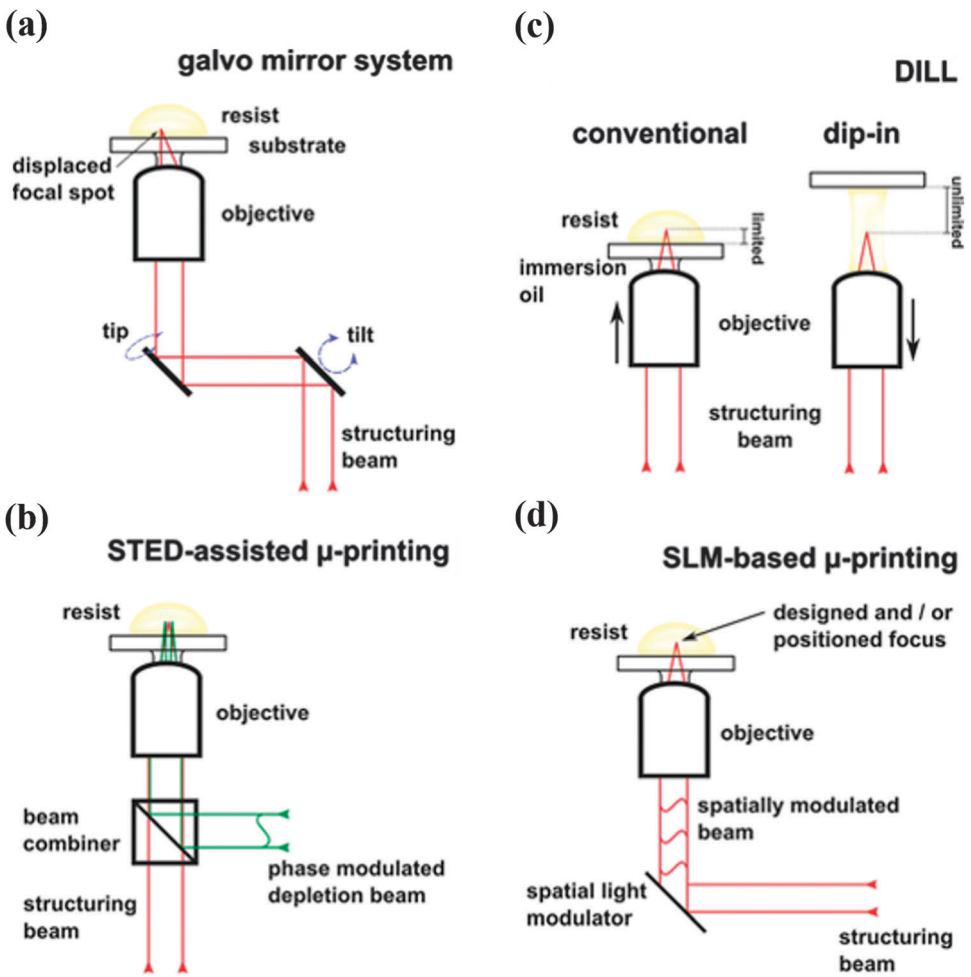

Fig. 11 Various schematics of direct laser writing (DLW): (a) galvanometric mirror-based DLW; (b) left: conventional DLW; right: dip-in DLW; (c) STED DLW; (d) SLM-based DLW. Reproduced with permission ref. 180. Copyright 2015, John Wiley and Sons.

 This journal is © The Royal Society of Chemistry 2016

Published on 18 April 2016. Downloaded by University of Texas Libraries on 14/06/2016 15:37:27.

which tilt the wave-front of the laser beam before it enters the objective, and therefore achieve accurate displacement of the focus spot of the laser beam (Fig. 11a). More recent developments include super-resolution writing, spatial-light-modulator-based writing, and the adoption of compact and less-expensive laser sources. Similar to the stimulated emission depletion (STED) microscopy,[186] super-resolution DLW uses two laser beams, *i.e.*, the structuring beam and the phase modulation depletion beam. The first beam is for resin polymerization, while the latter one is for turning the above polymerization process 'on' and 'off' (Fig. 11c). STED direct writing breaks the light diffraction limit and further improves the patterning resolution.[187] In spatial light modulator (SLM)-based writing, the SLM modulates the wave-front of the incident laser beam on a pixel basis before it enters the pupil of the focusing objective, and thus, achieves beam steering, aberration correction, and parallel writing at the same time (Fig. 11d).[188,189] To reduce costs, laser diodes have recently been employed, and have shown similar writing resolutions to those achieved by complex conventional systems.[190,191] Commercial DLW systems are available from vendors such as Nanoscribe, World of Photonics, and Newport.

DLW enables the creation of various complex 3D photonic structures, many of which cannot be easily fabricated by other lithography techniques (Fig. 12). For example, 3D helical metamaterials can be fabricated through a process based on DLW combined with gold plating (Fig. 12a).[192] Here, first, the helical polymer cast is created by DLW. The voids in the polymer cast are then filled with gold through electrochemical deposition. The remaining polymer template is finally removed by an oxygen plasma etching. Such devices work as compact IR broadband circular polarizers by blocking circularly polarized light with the same handedness as the helices, while transmitting circularly polarized light of the opposite handedness. Being able to control light beam propagation at will is useful for many integrated photonic devices. DLW has been used to fabricate spatially-variant photonic crystals (SVPCs) in SU-8, whereby the fabricated device can bend the flow of light around a 90° turn (Fig. 12b).[193] To accomplish this, the lattice spacing and fill factor remain nearly constant throughout the structure, but the orientation of adjacent unit cells is progressively rotated in order to gradually guide the flow of light. 3D optical interconnects are useful for on-chip optical devices, but are not easily fabricated by planar lithography techniques, such as photolithography, Ebeam lithography, and NIL. In contrast, DLW is powerful for creating such 3D structures, and indeed, it can be combined with the aforementioned planar patterning techniques to fabricate various 2D/3D hybrid optical devices, such as inter-chip photonic wire bonds[194] and on-chip polarization rotators[195] (Fig. 12c and d).

4.2 Dip-pen nanolithography

Dip-pen nanolithography (DPN) was proposed by Chad Mirkin and co-workers in 1999.[15] It is one kind of the scanning tip lithography,[16] and employs atomic force microscope (AFM) tips to deliver materials to the substrates *via* capillary transport (Fig. 13a).

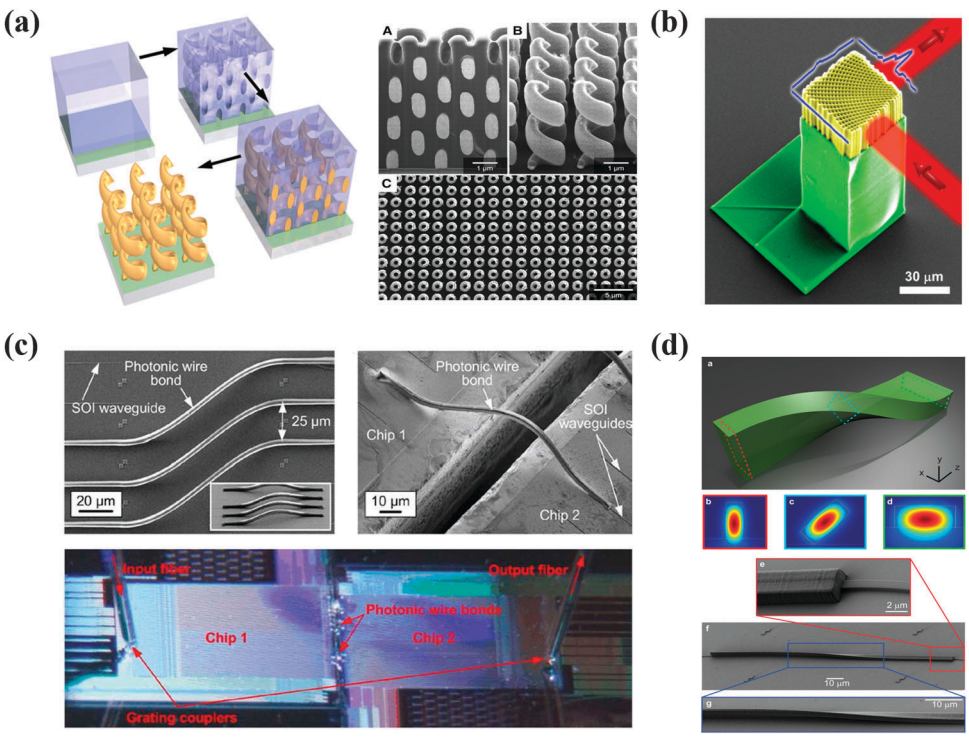

Fig. 12 Various photonic devices fabricated by DLW: (a) left: schematic of gold helical wire fabrication using DTW and gold plating; right: SEM of the fabricated structure. Reproduced with permission ref. 192. Copyright 2009, The American Association for the Advancement of Science. (b) False color SEM of spatially-variant photonic crystals for directing the flow of light through a 90° turn. Reproduced with permission ref. 193. Copyright 2014, Optical Society of America. (c) Inter-chip photonic wire bond fabricated by DLW. Reproduced with permission ref. 194. Copyright 2012, Optical Society of America. (d) Mode evolution-based polarization rotator fabricated by DLW. Reproduced with permission ref. 195. Copyright 2014, Nature Publishing Group.

Published on 18 April 2016. Downloaded by University of Texas Libraries on 14/06/2016 15:37:27.

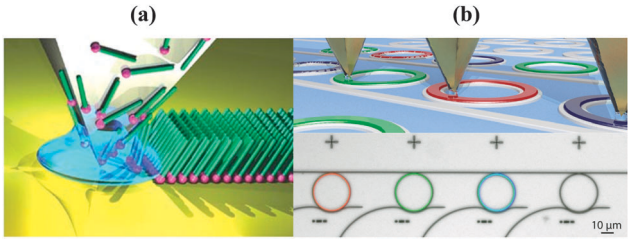

Fig. 13 (a) Schematic of DPN, which employs an AFM tip to deliver materials to the substrate *via* capillary transport. Reproduced with permission ref. 14. Copyright 2007, Nature Publishing Group. (b) Schematic of using DPN to "decorate" a diamond integrated optical circuit using lipid mixtures (top), together with the fluorescent microscope micrograph showing the result of three rings functionalized at the same time with three different fluorescent inks using DPN (bottom). Reproduced with permission ref. 197. Copyright 2014, John Wiley and Sons.

The deposited materials can be either molecular inks typically made of small molecules, which are coated onto the DPN tip and delivered to the surface through a water meniscus; or liquid inks, which can be any material that is in liquid form during deposition. Besides being directly used as a part of the devices, these deposited materials can also act as etching masks to transfer patterns to the layers beneath.[196]

Compared with other lithography techniques, such as photolithography and NIL, DPN is a rather slow process, except when massive AFM tips are used to write on a substrate simultaneously. However, DPN is attractive for quick prototyping, since it is a mask-less process performed in an ambient environment. Moreover, DPN can directly print various materials onto existing nano- and micro-structures with nano-scale registrations, and the substrates can be any material (including soft or insulating ones). Although DPN is not widely used to fabricate photonic devices, it can be combined with other lithography techniques to "decorate" exiting structures in a site-specific fashion. For example, DPN is employed for the functionalization of wafer-scale diamond integrated optical circuits using lipid mixtures, with a resolution down to 100 nm.[197] Here, transparent diamond thin films are first deposited on oxidized silicon wafers by chemical vapor deposition (CVD), resulting in diamond-on-insulator wafers. Ebeam lithography and reactive ion etching (RIE) are then applied to fabricate the ring resonators on these wafers. Afterwards, the DPN tips are used in parallel to modify the surfaces of several rings together. Finally, 4 nm high, curved florescent lipid lines are written on the waveguides, and these waveguides are evaluated by fluorescence measurements (Fig. 13b). Such a method enables a site-specific surface modification (coloring) of nanophotonic systems, without the need to immerse the entire device in liquid solutions.

4.3 Combining imprinting with other lithography techniques

The functionalities of NIL can be further enhanced by combining it with other lithography techniques. The continuous R2R fabrication of photonic devices can be envisioned by utilizing various lithography techniques, as shown in the schematics of Fig. 14. Here, photolithography and ink-jet printing are employed to fabricate micro-scale features, and NIL is then used to pattern both the micro- and nano-scale ones. Laser direct writing and Dip-pen nanolithography can be used for "decorating" the fabricated devices by adding 3D structures, inter-chip optical connects, *etc.* With the aid of alignment marks as well as quality inspections between steps, reasonable alignment accuracies and layer qualities can be assured. The development of such a high-rate manufacturing process enables a new suite of high-performance, lightweight, and low-cost integrated photonic systems to be developed.

5. Conclusions

Nanoimprinting provides a viable solution for fabricating high-performance and low-cost micro-/nano-scale photonic devices using a variety of materials on different substrates. By carefully preparing the imprint molds, the fabricated structures can be made with good profiles and smooth side-walls, which contribute to the manufacturing of low-loss optical interconnects and high quality factor optical resonators. Also, imprinting is capable of processing various materials, including thermoplastic polymers, UV-curable resins, and even metals. To move toward fast processing speeds, roll-to-roll (R2R)-based imprinting has been developed; and such a R2R processing scheme can be further enhanced by combining imprinting with other complementary lithography methods. It is worth studying how to incorporate these new schemes into the existing product manufacturing process. In the future, imprinting will continually be utilized to realize various designs of emerging photonic devices. At the same time, new imprinting resists as well as process schemes are to be investigated. In the case of imprinting resists, for example, materials with simpler imprinting requirements, better etching robustness, and improved or new functionalities are desired. Imprinting schemes with faster processing speed, better overlay accuracies, and less

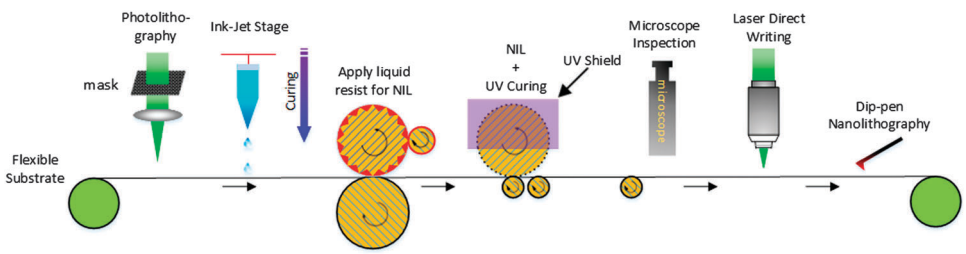

Fig. 14 Schematic of a continuous R2R fabrication process for photonic devices utilizing various lithography methods.

 This journal is © The Royal Society of Chemistry 2016

Published on 18 April 2016. Downloaded by University of Texas Libraries on 14/06/2016 15:37:27.

defect generations are currently being developed. Printed photonic components and even complete circuits can be envisioned in the future.

Acknowledgements

The authors acknowledge the financial support from National Science Foundation (NSF) under grant number DMR 1120187, CMMI 1025020 and DBI 1256001, as well as Air Force Office of Scientific Research (AFOSR) under grant number FA9550-14-C-0001. J. G. Ok acknowledges the financial support from National Research Foundation of Korea under grant number 2015R1A5A1037668 and Samsung Display, Co., Ltd. The authors acknowledge the technical support from Lurie Nanofabrication Facility (LNF) at the University of Michigan.

References

1 C. Mack, Introduction to Semiconductor Lithography, *Fundamental Principles of Optical Lithography*, John Wiley & Sons, Ltd, 2007, pp. 1–28.
2 M. Totzeck, W. Ulrich, A. Gohnermeier and W. Kaiser, Semiconductor fabrication: pushing deep ultraviolet lithography to its limits, *Nat. Photonics*, 2007, **1**, 629–631.
3 B. Wu and A. Kumar, Extreme ultraviolet lithography: a review, *J. Vac. Sci. Technol., B: Microelectron. Nanometer Struct.–Process., Meas., Phenom.*, 2007, **25**, 1743–1761.
4 M. C. Peckerar and J. R. Maldonado, X-ray lithography-an overview, *Proc. IEEE*, 1993, **81**, 1249–1274.
5 L. Pan, Y. Park, Y. Xiong, E. Ulin-Avila, Y. Wang and L. Zeng, *et al.*, Maskless Plasmonic Lithography at 22 nm Resolution, *Sci. Rep.*, 2011, **1**, 175.
6 X. Chen, F. Yang, C. Zhang, J. Zhou and L. J. Guo, Large-Area High Aspect Ratio Plasmonic Interference Lithography Utilizing a Single High-k Mode, *ACS Nano*, 2016, **10**, 4039–4045, DOI: 10.1021/acsnano.5b06137.
7 Y. Chen, Nanofabrication by electron beam lithography and its applications: a review, *Microelectron. Eng.*, 2015, **135**, 57–72.
8 M. Altissimo, E-beam lithography for micro-/nanofabrication, *Biomicrofluidics*, 2010, **4**, 026503.
9 K. Arshak, M. Mihov, A. Arshak, D. McDonagh and D. Sutton, Focused ion beam lithography-overview and new approaches, in *Microelectronics, 2004. 24th International Conference on*, 2004, vol. 2, pp. 459–462.
10 L. J. Guo, Nanoimprint Lithography: Methods and Material Requirements, *Adv. Mater.*, 2007, **19**, 495–513.
11 S. Alom Ruiz and C. S. Chen, Microcontact printing: a tool to pattern, *Soft Matter*, 2007, **3**, 168–177.
12 A. Perl, D. N. Reinhoudt and J. Huskens, Microcontact Printing: Limitations and Achievements, *Adv. Mater.*, 2009, **21**, 2257–2268.
13 M. Deubel, G. von Freymann, M. Wegener, S. Pereira, K. Busch and C. M. Soukoulis, Direct laser writing of three-dimensional photonic-crystal templates for telecommunications, *Nat. Mater.*, 2004, **3**, 444–447.
14 K. Salaita, Y. Wang and C. A. Mirkin, Applications of dip-pen nanolithography, *Nat. Nanotechnol.*, 2007, **2**, 145–155.
15 R. D. Piner, J. Zhu, F. Xu, S. Hong and C. A. Mirkin, Dip-Pen Nanolithography, *Science*, 1999, **283**, 661–663.
16 R. Garcia, A. W. Knoll and E. Riedo, Advanced scanning probe lithography, *Nat. Nanotechnol.*, 2014, **9**, 577–587.
17 G. A. Ozin, K. Hou, B. V. Lotsch, L. Cademartiri, D. P. Puzzo and F. Scotognella, *et al.*, Nanofabrication by self-assembly, *Mater. Today*, 2009, **12**, 12–23.
18 C. A. Ross, K. K. Berggren, J. Y. Cheng, Y. S. Jung and J.-B. Chang, Three-Dimensional Nanofabrication by Block Copolymer Self-Assembly, *Adv. Mater.*, 2014, **26**, 4386–4396.
19 S. Y. Chou, P. R. Krauss and P. J. Renstrom, Imprint of sub-25 nm vias and trenches in polymers, *Appl. Phys. Lett.*, 1995, **67**, 3114–3116.
20 S. Y. Chou, P. R. Krauss and P. J. Renstrom, Imprint Lithography with 25-Nanometer Resolution, *Science*, 1996, **272**, 85–87.
21 F. Susumu, Fine Pattern Fabrication by the Molded Mask Method (Nanoimprint Lithography) in the 1970s, *Jpn. J. Appl. Phys.*, 2009, **48**, 06FH01.
22 M. Colburn, S. C. Johnson, M. D. Stewart, S. Damle, T. C. Bailey and B. Choi, *et al.*, Step and flash imprint lithography: a new approach to high-resolution patterning, *Proc. SPIE*, 1999, **3676**, 379, DOI: 10.1117/12.351155.
23 G. M. Schmid, M. Miller, C. Brooks, N. Khusnatdinov, D. LaBrake and D. J. Resnick, *et al.*, Step and flash imprint lithography for manufacturing patterned media, *J. Vac. Sci. Technol., B: Microelectron. Nanometer Struct.–Process., Meas., Phenom.*, 2009, **27**, 573–580.
24 S. Y. Chou, P. R. Krauss, W. Zhang, L. Guo and L. Zhuang, Sub-10 nm imprint lithography and applications, *J. Vac. Sci. Technol., B: Microelectron. Nanometer Struct.–Process., Meas., Phenom.*, 1997, **15**, 2897–2904.
25 X. Liang, W. Zhang, M. Li, Q. Xia, W. Wu and H. Ge, *et al.*, Electrostatic Force-Assisted Nanoimprint Lithography (EFAN), *Nano Lett.*, 2005, **5**, 527–530.
26 H. Yoshihiko, H. Satoshi, I. Satoshi, K. Michio and T. Yoshio, Nano-Imprint Lithography Using Replicated Mold by Ni Electroforming, *Jpn. J. Appl. Phys.*, 2002, **41**, 4186.
27 B. D. Gates, Q. Xu, M. Stewart, D. Ryan, C. G. Willson and G. M. Whitesides, New Approaches to Nanofabrication: Molding, Printing and Other Techniques, *Chem. Rev.*, 2005, **105**, 1171–1196.
28 T. W. Odom, J. C. Love, D. B. Wolfe, K. E. Paul and G. M. Whitesides, Improved Pattern Transfer in Soft Lithography Using Composite Stamps, *Langmuir*, 2002, **18**, 5314–5320.
29 H. Schmid and B. Michel, Siloxane Polymers for High-Resolution, High-Accuracy Soft Lithography, *Macromolecules*, 2000, **33**, 3042–3049.
30 T. W. Odom, V. R. Thalladi, J. C. Love and G. M. Whitesides, Generation of 30–50 nm Structures Using Easily Fabricated, Composite PDMS Masks, *J. Am. Chem. Soc.*, 2002, **124**, 12112–12113.

Published on 18 April 2016. Downloaded by University of Texas Libraries on 14/06/2016 15:37:27.

31 J. P. Rolland, E. C. Hagberg, G. M. Denison, K. R. Carter and J. M. De Simone, High-Resolution Soft Lithography: Enabling Materials for Nanotechnologies, *Angew. Chem., Int. Ed.*, 2004, **43**, 5796–5799.
32 J. P. Rolland, R. M. Van Dam, D. A. Schorzman, S. R. Quake and J. M. DeSimone, Solvent-Resistant Photocurable Liquid Teflon for Microfluidic Device Fabrication, *J. Am. Chem. Soc.*, 2004, **126**, 2322–2323.
33 S. S. Williams, S. Retterer, R. Lopez, R. Ruiz, E. T. Samulski and J. M. DeSimone, High-Resolution PFPE-based Molding Techniques for Nanofabrication of High-Pattern Density, Sub-20 nm Features: A Fundamental Materials Approach, *Nano Lett.*, 2010, **10**, 1421–1428.
34 S.-J. Choi, P. J. Yoo, S. J. Baek, T. W. Kim and H. H. Lee, An Ultraviolet-Curable Mold for Sub-100-nm Lithography, *J. Am. Chem. Soc.*, 2004, **126**, 7744–7745.
35 D. Matsukawa, H. Wakayama, K. Mitsukura, H. Okamura, Y. Hirai and M. Shirai, A UV curable resin with reworkable properties: application to imprint lithography, *J. Mater. Chem.*, 2009, **19**, 4085–4087.
36 C. Lu and R. H. Lipson, Interference lithography: a powerful tool for fabricating periodic structures, *Laser Photonics Rev.*, 2010, **4**, 568–580.
37 A. Bagal and C.-H. Chang, Fabrication of subwavelength periodic nanostructures using liquid immersion Lloyd's mirror interference lithography, *Opt. Lett.*, 2013, **38**, 2531–2534.
38 M.-G. Kang, M.-S. Kim, J. Kim and L. J. Guo, Organic Solar Cells Using Nanoimprinted Transparent Metal Electrodes, *Adv. Mater.*, 2008, **20**, 4408–4413.
39 B. Cui, Z. Yu, H. Ge and S. Y. Chou, Large area 50 nm period grating by multiple nanoimprint lithography and spatial frequency doubling, *Appl. Phys. Lett.*, 2007, **90**, 043118.
40 E. Lepore and N. Pugno, Superhydrophobic Polystyrene by Direct Copy of a Lotus Leaf, *Bionanoscience*, 2011, **1**, 136–143.
41 G. Zhang, J. Zhang, G. Xie, Z. Liu and H. Shao, Cicada Wings: A Stamp from Nature for Nanoimprint Lithography, *Small*, 2006, **2**, 1440–1443.
42 A. J. Smith, C. Wang, D. Guo, C. Sun and J. Huang, Repurposing Blu-ray movie discs as quasi-random nanoimprinting templates for photon management, *Nat. Commun.*, 2014, **5**, 5517.
43 H. J. Ensikat, P. Ditsche-Kuru, C. Neinhuis and W. Barthlott, Superhydrophobicity in perfection: the outstanding properties of the lotus leaf, *Beilstein J. Nanotechnol.*, 2011, **2**, 152–161.
44 C.-Y. Chao and L. J. Guo, Thermal-flow technique for reducing surface roughness and controlling gap size in polymer microring resonators, *Appl. Phys. Lett.*, 2004, **84**, 2479–2481.
45 T. Ling, S.-L. Chen and L. J. Guo, Fabrication and characterization of High *Q* polymer micro-ring resonator and its application as a sensitive ultrasonic detector, *Opt. Express*, 2011, **19**, 861–869.
46 S. Y. Chou and Q. Xia, Improved nanofabrication through guided transient liquefaction, *Nat. Nanotechnol.*, 2008, **3**, 295–300.
47 M. Beck, M. Graczyk, I. Maximov, E. L. Sarwe, T. G. I. Ling and M. Keil, *et al.*, Improving stamps for 10 nm level wafer scale nanoimprint lithography, *Microelectron. Eng.*, 2002, **61–62**, 441–448.
48 L. J. Guo, Recent progress in nanoimprint technology and its applications, *J. Phys. D: Appl. Phys.*, 2004, **37**, R123.
49 P. Ruchhoeft, M. Colburn, B. Choi, H. Nounu, S. Johnson and T. Bailey, *et al.*, Patterning curved surfaces: template generation by ion beam proximity lithography and relief transfer by step and flash imprint lithography, *J. Vac. Sci. Technol., B: Microelectron. Nanometer Struct.–Process., Meas., Phenom.*, 1999, **17**, 2965–2969.
50 R. Ji, M. Hornung, M. A. Verschuuren, R. van de Laar, J. van Eekelen and U. Plachetka, *et al.*, UV enhanced substrate conformal imprint lithography (UV-SCIL) technique for photonic crystals patterning in LED manufacturing, *Microelectron. Eng.*, 2010, **87**, 963–967.
51 L.-R. Bao, X. Cheng, X. D. Huang, L. J. Guo, S. W. Pang and A. F. Yee, Nanoimprinting over topography and multilayer three-dimensional printing, *J. Vac. Sci. Technol., B: Microelectron. Nanometer Struct.–Process., Meas., Phenom.*, 2002, **20**, 2881–2886.
52 N. Kehagias, V. Reboud, G. Chansin, M. Zelsmann, C. Jeppesen and C. Schuster, *et al.*, Reverse-contact UV nanoimprint lithography for multilayered structure fabrication, *Nanotechnology*, 2007, **18**, 175303.
53 P. Nagpal, N. C. Lindquist, S.-H. Oh and D. J. Norris, Ultrasmooth Patterned Metals for Plasmonics and Metamaterials, *Science*, 2009, **325**, 594–597.
54 D. Lin, H. Tao, J. Trevino, J. P. Mondia, D. L. Kaplan and F. G. Omenetto, *et al.*, Direct Transfer of Subwavelength Plasmonic Nanostructures on Bioactive Silk Films, *Adv. Mater.*, 2012, **24**, 6088–6093.
55 M.-G. Kang and L. J. Guo, Metal transfer assisted nanolithography on rigid and flexible substrates, *J. Vac. Sci. Technol., B: Microelectron. Nanometer Struct.–Process., Meas., Phenom.*, 2008, **26**, 2421–2425.
56 X. Cheng and L. Jay Guo, One-step lithography for various size patterns with a hybrid mask-mold, *Microelectron. Eng.*, 2004, **71**, 288–293.
57 X. Cheng and L. Jay Guo, A combined-nanoimprint-and-photolithography patterning technique, *Microelectron. Eng.*, 2004, **71**, 277–282.
58 S. Buzzi, F. Robin, V. Callegari and J. F. Löffler, Metal direct nanoimprinting for photonics, *Microelectron. Eng.*, 2008, **85**, 419–424.
59 S. Buzzi, M. Galli, M. Agio and J. F. Löffler, Silver high-aspect-ratio micro- and nanoimprinting for optical applications, *Appl. Phys. Lett.*, 2009, **94**, 223115.
60 L. T. Varghese, L. Fan, Y. Xuan, C. Tansarawiput, S. Kim and M. Qi, Resistless Nanoimprinting in Metal for Plasmonic Nanostructures, *Small*, 2013, **9**, 3778–3783.
61 S. Y. Chou, C. Keimel and J. Gu, Ultrafast and direct imprint of nanostructures in silicon, *Nature*, 2002, **417**, 835–837.
62 C. Bo, K. Chris and Y. C. Stephen, Ultrafast direct imprinting of nanostructures in metals by pulsed laser melting, *Nanotechnology*, 2010, **21**, 045303.

 This journal is © The Royal Society of Chemistry 2016

Published on 18 April 2016. Downloaded by University of Texas Libraries on 14/06/2016 15:37:27.

63 J. G. Ok, S. H. Ahn, M. K. Kwak and L. J. Guo, Continuous and high-throughput nanopatterning methodologies based on mechanical deformation, *J. Mater. Chem. C*, 2013, **1**, 7681–7691.

64 J. G. Ok, H. Seok Youn, M. Kyu Kwak, K.-T. Lee, Y. Jae Shin and L. Jay Guo, *et al.*, Continuous and scalable fabrication of flexible metamaterial films *via* roll-to-roll nanoimprint process for broadband plasmonic infrared filters, *Appl. Phys. Lett.*, 2012, **101**, 223102.

65 J. G. Ok, M. K. Kwak, C. M. Huard, H. S. Youn and L. J. Guo, Photo–Roll Lithography (PRL) for Continuous and Scalable Patterning with Application in Flexible Electronics, *Adv. Mater.*, 2013, **25**, 6554–6561.

66 S. H. Ahn, J.-S. Kim and L. J. Guo, Bilayer metal wire-grid polarizer fabricated by roll-to-roll nanoimprint lithography on flexible plastic substrate, *J. Vac. Sci. Technol., B: Microelectron. Nanometer Struct.–Process., Meas., Phenom.*, 2007, **25**, 2388–2391.

67 H.-H. Lin, C.-h. Lee and M.-H. Lu, Dye-less color filter fabricated by roll-to-roll imprinting for liquid crystal display applications, *Opt. Express*, 2009, **17**, 12397–12406.

68 H. J. Park, M.-G. Kang, S. H. Ahn and L. J. Guo, A Facile Route to Polymer Solar Cells with Optimum Morphology Readily Applicable to a Roll-to-Roll Process without Sacrificing High Device Performances, *Adv. Mater.*, 2010, **22**, E247–E253.

69 F. C. Krebs, T. Tromholt and M. Jorgensen, Upscaling of polymer solar cell fabrication using full roll-to-roll processing, *Nanoscale*, 2010, **2**, 873–886.

70 H. Zhu, Z. Fang, C. Preston, Y. Li and L. Hu, Transparent paper: fabrications, properties and device applications, *Energy Environ. Sci.*, 2014, **7**, 269–287.

71 R. R. Søndergaard, M. Hösel and F. C. Krebs, Roll-to-roll fabrication of large area functional organic materials, *J. Polym. Sci., Part B: Polym. Phys.*, 2013, **51**, 16–34.

72 S. H. Ahn and L. J. Guo, Dynamic Nanoinscribing for Continuous and Seamless Metal and Polymer Nanogratings, *Nano Lett.*, 2009, **9**, 4392–4397.

73 S. H. Ahn, J. G. Ok, M. K. Kwak, K.-T. Lee, J. Y. Lee and L. J. Guo, Template-Free Vibrational Indentation Patterning (VIP) of Micro/Nanometer-Scale Grating Structures with Real-Time Pitch and Angle Tunability, *Adv. Funct. Mater.*, 2013, **23**, 4739–4744.

74 J. G. Ok, A. Panday, T. Lee and L. Jay Guo, Continuous fabrication of scalable 2-dimensional (2D) micro- and nanostructures by sequential 1D mechanical patterning processes, *Nanoscale*, 2014, **6**, 14636–14642.

75 P.-H. Carlos, K. Alexander, D. Lucas, D. Scott, P. Aleksandr and C. Giuseppe, *et al.*, Printable planar lightwave circuits with a high refractive index, *Nanotechnology*, 2014, **25**, 325302.

76 J. Landwehr, R. Fader, M. Rumler, M. Rommel, A. J. Bauer and L. Frey, *et al.*, Optical polymers with tunable refractive index for nanoimprint technologies, *Nanotechnology*, 2014, **25**, 505301.

77 M. Tamborra, M. Striccoli, M. L. Curri, J. A. Alducin, D. Mecerreyes and J. A. Pomposo, *et al.*, Nanocrystal-Based Luminescent Composites for Nanoimprinting Lithography, *Small*, 2007, **3**, 822–828.

78 V. Reboud, T. Kehoe, J. Romero Vivas, N. Kehagias, M. Zelsmann and F. Alsina, *et al.*, Polymer photonic band-gaps fabricated by nanoimprint lithography, *Photonics and Nanostructures – Fundamentals and Applications*, 2012, **10**, 632–635.

79 C. Battaglia, K. Söderström, J. Escarre and F.-J. Haug, *et al.*, Nanomoulding of Functional Materials, a Versatile Complementary Pattern Replication Method to Nanoimprinting, *J. Visualized Exp.*, 2013, e50177.

80 S. Y. Chou, P. R. Krauss and P. J. Renstrom, Nanoimprint lithography, *J. Vac. Sci. Technol., B: Microelectron. Nanometer Struct.–Process., Meas., Phenom.*, 1996, **14**, 4129–4133.

81 C. Zhang, T. Ling, S.-L. Chen and L. J. Guo, Ultrabroad Bandwidth and Highly Sensitive Optical Ultrasonic Detector for Photoacoustic Imaging, *ACS Photonics*, 2014, **1**, 1093–1098.

82 C.-y. Chao and L. J. Guo, Polymer microring resonators fabricated by nanoimprint technique, *J. Vac. Sci. Technol., B: Microelectron. Nanometer Struct.–Process., Meas., Phenom.*, 2002, **20**, 2862–2866.

83 P. Corinne, G. Cécile, M. Guillaume and G. Jean Pierre, Influence of Thermal Properties of Polymers on Nano-Imprint Lithography Performance, *Jpn. J. Appl. Phys.*, 2002, **41**, 4203.

84 C. Con, J. Zhang, Z. Jahed, T. Y. Tsui, M. Yavuz and B. Cui, Thermal nanoimprint lithography using fluoropolymer mold, *Microelectron. Eng.*, 2012, **98**, 246–249.

85 T. Nielsen, D. Nilsson, F. Bundgaard, P. Shi, P. Szabo and O. Geschke, *et al.*, Nanoimprint lithography in the cyclic olefin copolymer, Topas®, a highly ultraviolet-transparent and chemically resistant thermoplast, *J. Vac. Sci. Technol., B: Microelectron. Nanometer Struct.–Process., Meas., Phenom.*, 2004, **22**, 1770–1775.

86 S.-W. Youn, A. Ueno, M. Takahashi and R. Maeda, Microstructuring of SU-8 photoresist by UV-assisted thermal imprinting with non-transparent mold, *Microelectron. Eng.*, 2008, **85**, 1924–1931.

87 L.-J. Cheng, M.-T. Kao, E. Meyhöfer and L. J. Guo, Highly Efficient Guiding of Microtubule Transport with Imprinted CYTOP Nanotracks, *Small*, 2005, **1**, 409–414.

88 J. Bian, T. Yang, C. Yuan, H. Ge and Y. Chen, Sub-50 nm UV-curing nanoimprint based on fluoropolymer, CYTOP, mold, *Appl. Phys. A: Mater. Sci. Process.*, 2013, **116**, 79–84.

89 X. Lin, T. Ling, H. Subbaraman, X. Zhang, K. Byun and L. J. Guo, *et al.*, Ultraviolet imprinting and aligned ink-jet printing for multilayer patterning of electro-optic polymer modulators, *Opt. Lett.*, 2013, **38**, 1597–1599.

90 M. Mühlberger, I. Bergmair, A. Klukowska, A. Kolander, H. Leichtfried and E. Platzgummer, *et al.*, UV-NIL with working stamps made from Ormostamp, *Microelectron. Eng.*, 2009, **86**, 691–693.

91 M. U. Khan, J. Justice, J. Petäjä, T. Korhonen, A. Boersma and S. Wiegersma, *et al.*, Multi-level single mode 2D polymer waveguide optical interconnects using nano-imprint lithography, *Opt. Express*, 2015, **23**, 14630–14639.

Published on 18 April 2016. Downloaded by University of Texas Libraries on 14/06/2016 15:37:27.

92 A. Khan, S. Li, X. Tang and W.-D. Li, Nanostructure transfer using cyclic olefin copolymer templates fabricated by thermal nanoimprint lithography, *J. Vac. Sci. Technol., B: Microelectron. Nanometer Struct.–Process., Meas., Phenom.*, 2014, **32**, 06FI02.
93 M. Horowitz, Y. Chih-Kong Ken and S. Sidiropoulos, High-speed electrical signaling: overview and limitations, *IEEE Micro*, 1998, **18**, 12–24.
94 N. P. Jouppi, Optical interconnects for high-performance computing systems, *Optical Interconnects Conference, 2012 IEEE*, 2012, pp. 31–31.
95 D. A. B. Miller, Physical Reasons for Optical Interconnects, *Int. J. OptoElectron.*, 1997, **11**, 155–168.
96 C. Sun, M. T. Wade, Y. Lee, J. S. Orcutt, L. Alloatti and M. S. Georgas, *et al.*, Single-chip microprocessor that communicates directly using light, *Nature*, 2015, **528**, 534–538.
97 W. H. Wong, K. K. Liu, K. S. Chan and E. Y. B. Pun, Polymer devices for photonic applications, *J. Cryst. Growth*, 2006, **288**, 100–104.
98 X. Zhang, A. Hosseini, X. Lin, H. Subbaraman and R. T. Chen, Polymer-Based Hybrid-Integrated Photonic Devices for Silicon On-Chip Modulation and Board-Level Optical Interconnects, *IEEE J. Sel. Top. Quantum Electron.*, 2013, **19**, 196–210.
99 M. B. Christiansen, M. Schøler and A. Kristensen, Integration of active and passive polymer optics, *Opt. Express*, 2007, **15**, 3931–3939.
100 H. Ma, A. K. Y. Jen and L. R. Dalton, Polymer-Based Optical Waveguides: Materials, Processing and Devices, *Adv. Mater.*, 2002, **14**, 1339–1365.
101 C.-Y. Lin, A. X. Wang, B. S. Lee, X. Zhang and R. T. Chen, High dynamic range electric field sensor for electromagnetic pulse detection, *Opt. Express*, 2011, **19**, 17372–17377.
102 X. Zhang, B. Lee, C. y. Lin, A. X. Wang, A. Hosseini and R. T. Chen, Highly Linear Broadband Optical Modulator Based on Electro-Optic Polymer, *IEEE Photonics J.*, 2012, **4**, 2214–2228.
103 K. Geary, K. Seong-Ku, S. Byoung-Joon, H. Yu-Chueh, Y. Wei and H. R. Fetterman, Photobleached refractive index tapers in electrooptic polymer rib waveguides, *IEEE Photonics Technol. Lett.*, 2006, **18**, 64–66.
104 H. K. Kim, S.-J. Kang, S.-K. Choi, Y.-H. Min and C.-S. Yoon, Highly Efficient Organic/Inorganic Hybrid Nonlinear Optic Materials *via* Sol–Gel Process: Synthesis, Optical Properties and Photobleaching for Channel Waveguides, *Chem. Mater.*, 1999, **11**, 779–788.
105 C. Zhang, S. Chen, T. Ling and L. J. Guo, Review of Imprinted Polymer Microrings as Ultrasound Detectors: Design, Fabrication and Characterization, *IEEE Sens. J.*, 2015, **15**, 3241–3248.
106 M. Wang, J. Hiltunen, S. Uusitalo, J. Puustinen, J. Lappalainen and P. Karioja, *et al.*, Fabrication of optical inverted-rib waveguides using UV-imprinting, *Microelectron. Eng.*, 2011, **88**, 175–178.
107 J. Hiltunen, A. Kokkonen, J. Puustinen, M. Hiltunen and J. Lappalainen, UV-Imprinted Single-Mode Waveguides With Low Loss at Visible Wavelength, *IEEE Photonics Technol. Lett.*, 2013, **25**, 996–998.
108 G. Calafiore, A. Koshelev, S. Dhuey, S. Sassolini, M. Messerschmidt and A. Schleunitz, *et al.*, Step-and-repeat nanoimprint on pre-spin coated film for the fabrication of integrated optical devices, *J. Micro/Nanolithogr., MEMS, MOEMS*, 2015, **14**, 033506.
109 C. Giuseppe, F. Quentin, D. Scott, S. Simone, S. Filippo and A. M. Camilo, *et al.*, Printable photonic crystals with high refractive index for applications in visible light, *Nanotechnology*, 2016, **27**, 115303.
110 B. Yun, G. Hu and Y. Cui, Polymer waveguide Bragg grating Fabry–Perot filter using a nanoimprinting technique, *J. Opt.*, 2014, **16**, 105501.
111 Z. Pan, H. Subbaraman, Y. Zou, X. Xu, X. Zhang and C. Zhang, *et al.*, Quasi-vertical tapers for polymer-waveguide-based interboard optical interconnects, *Photonics Res.*, 2015, **3**, 317–323.
112 X. Zhang, H. Subbaraman, A. Hosseini and R. T. Chen, Highly efficient mode converter for coupling light into wide slot photonic crystal waveguide, *Opt. Express*, 2014, **22**, 20678–20690.
113 C. T. Chen, X. Xu, A. Hosseini, Z. Pan, H. Subbaraman and X. Zhang, *et al.*, Design of Highly Efficient Hybrid Si–Au Taper for Dielectric Strip Waveguide to Plasmonic Slot Waveguide Mode Converter, *J. Lightwave Technol.*, 2015, **33**, 535–540.
114 X. Lin, T. Ling, H. Subbaraman, L. J. Guo and R. T. Chen, Printable thermo-optic polymer switches utilizing imprinting and ink-jet printing, *Opt. Express*, 2013, **21**, 2110–2117.
115 Z. Pan, H. Subbaraman, C. Zhang, A. Panday, Q. Li and X. Zhang, *et al.*, Reconfigurable thermo-optic polymer switch based true-time-delay network utilizing imprinting and inkjet printing, *Proc. SPIE*, 2015, **9362**, 936214, DOI: 10.1117/12.2080115.
116 X. Zhang, C. j. Chung, A. Hosseini, H. Subbaraman, J. Luo and A. Jen, *et al.*, High Performance Optical Modulator Based on Electro-optic Polymer Filled Silicon Slot Photonic Crystal Waveguide, *J. Lightwave Technol.*, 2015, 1.
117 D. Chen, H. R. Fetterman, A. Chen, W. H. Steier, L. R. Dalton and W. Wang, *et al.*, Demonstration of 110 GHz electro-optic polymer modulators, *Appl. Phys. Lett.*, 1997, **70**, 3335–3337.
118 M. Lee, H. E. Katz, C. Erben, D. M. Gill, P. Gopalan and J. D. Heber, *et al.*, Broadband Modulation of Light by Using an Electro-Optic Polymer, *Science*, 2002, **298**, 1401–1403.
119 X. Zhang, A. Hosseini, H. Subbaraman, S. Wang, Q. Zhan and J. Luo, *et al.*, Integrated Photonic Electromagnetic Field Sensor Based on Broadband Bowtie Antenna Coupled Silicon Organic Hybrid Modulator, *J. Lightwave Technol.*, 2014, **32**, 3774–3784.
120 B. Guha, K. Preston and M. Lipson, Athermal silicon microring electro-optic modulator, *Opt. Lett.*, 2012, **37**, 2253–2255.
121 S. Rao, G. Coppola, M. A. Gioffrè and F. G. Della Corte, A 2.5 ns switching time Mach–Zehnder modulator in as-deposited a-Si:H, *Opt. Express*, 2012, **20**, 9351–9356.

 This journal is © The Royal Society of Chemistry 2016

Published on 18 April 2016. Downloaded by University of Texas Libraries on 14/06/2016 15:37:27.

122 Y. Liu and H. W. M. Salemink, Photonic crystal-based all-optical on-chip sensor, *Opt. Express*, 2012, **20**, 19912–19920.
123 C. Fenzl, T. Hirsch and O. S. Wolfbeis, Photonic Crystals for Chemical Sensing and Biosensing, *Angew. Chem., Int. Ed.*, 2014, **53**, 3318–3335.
124 X. Zhang, G. Zhou, P. Shi, H. Du, T. Lin and J. Teng, *et al.*, On-chip integrated optofluidic complex refractive index sensing using silicon photonic crystal nanobeam cavities, *Opt. Lett.*, 2016, **41**, 1197–1200.
125 J. N. Anker, W. P. Hall, O. Lyandres, N. C. Shah, J. Zhao and R. P. Van Duyne, Biosensing with plasmonic nanosensors, *Nat. Mater.*, 2008, **7**, 442–453.
126 M. E. Stewart, C. R. Anderton, L. B. Thompson, J. Maria, S. K. Gray and J. A. Rogers, *et al.*, Nanostructured Plasmonic Sensors, *Chem. Rev.*, 2008, **108**, 494–521.
127 X. Xu, B. Peng, D. Li, J. Zhang, L. M. Wong and Q. Zhang, *et al.*, Flexible Visible-Infrared Metamaterials and Their Applications in Highly Sensitive Chemical and Biological Sensing, *Nano Lett.*, 2011, **11**, 3232–3238.
128 H. Tao, E. A. Kadlec, A. C. Strikwerda, K. Fan, W. J. Padilla and R. D. Averitt, *et al.*, Microwave and terahertz wave sensing with metamaterials, *Opt. Express*, 2011, **19**, 21620–21626.
129 I. M. White, H. Oveys and X. Fan, Liquid-core optical ring-resonator sensors, *Opt. Lett.*, 2006, **31**, 1319–1321.
130 C. Zhang, S.-L. Chen, T. Ling and L. J. Guo, Imprinted Polymer Microrings as High-Performance Ultrasound Detectors in Photoacoustic Imaging, *J. Lightwave Technol.*, 2015, **33**, 4318–4328.
131 X. Zhang, L. Liu and L. Xu, Ultralow sensing limit in optofluidic micro-bottle resonator biosensor by self-referenced differential-mode detection scheme, *Appl. Phys. Lett.*, 2014, **104**, 033703.
132 C.-Y. Chao and L. J. Guo, Biochemical sensors based on polymer microrings with sharp asymmetrical resonance, *Appl. Phys. Lett.*, 2003, **83**, 1527–1529.
133 T. Sünner, T. Stichel, S.-H. Kwon, T. W. Schlereth, S. Höfling and M. Kamp, *et al.*, Photonic crystal cavity based gas sensor, *Appl. Phys. Lett.*, 2008, **92**, 261112.
134 Q. Chen, X. Zhang, Y. Sun, M. Ritt, S. Sivaramakrishnan and X. Fan, Highly sensitive fluorescent protein FRET detection using optofluidic lasers, *Lab Chip*, 2013, **13**, 2679–2681.
135 S.-L. Chen, H. Sheng-Wen, L. Tao, S. Ashkenazi and L. J. Guo, Polymer microring resonators for high-sensitivity and wideband photoacoustic imaging, *IEEE Transactions on Ultrasonics, Ferroelectrics and Frequency Control*, 2009, **56**, 2482–2491.
136 S.-L. Chen, T. Ling and L. J. Guo, Low-noise small-size microring ultrasonic detectors for high-resolution photoacoustic imaging, *J. Biomed. Opt.*, 2011, **16**, 056001.
137 C.-T. Wang, C.-Y. Wang, J.-H. Yu, I. T. Kuo, C.-W. Tseng and H.-C. Jau, *et al.*, Highly sensitive optical temperature sensor based on a SiN micro-ring resonator with liquid crystal cladding, *Opt. Express*, 2016, **24**, 1002–1007.
138 S.-L. Chen, C. Zhang, Y.-C. Chang, J. G. Ok, T. Ling and M. T. Mihnev, *et al.*, Efficient Real-time Detection of Terahertz Pulse Radiation by Listening to Photoacoustic Generation, *Frontiers in Optics 2014*, Tucson, Arizona, 2014, p. LTh4I.1.
139 J. E. Heebner, R. Grover and T. A. Ibrahim, *Optical microresonators: theory, fabrication and applications*, Springer, London, 2008.
140 T. Ling, S.-L. Chen and L. J. Guo, High-sensitivity and wide-directivity ultrasound detection using high *Q* polymer microring resonators, *Appl. Phys. Lett.*, 2011, **98**, 204103.
141 B. E. A. Saleh and T. Malvin Carl, *Fundamentals of photonics*, Wiley-interscience, 2007.
142 Z. Xie, S.-L. Chen, T. Ling, L. J. Guo, P. L. Carson and X. Wang, Pure optical photoacoustic microscopy, *Opt. Express*, 2011, **19**, 9027–9034.
143 S.-L. Chen, Z. Xie, T. Ling, L. Jay Guo, X. Wei and X. Wang, Miniaturized all-optical photoacoustic microscopy based on microelectromechanical systems mirror scanning, *Opt. Lett.*, 2012, **37**, 4263–4265.
144 S.-L. Chen, Y.-C. Chang, C. Zhang, J. G. Ok, T. Ling and M. T. Mihnev, *et al.*, Efficient real-time detection of terahertz pulse radiation based on photoacoustic conversion by carbon nanotube nanocomposite, *Nat. Photonics*, 2014, **8**, 537.
145 C. Zhang, D. Zhao, D. Gu, H. Kim, T. Ling and Y.-K. R. Wu, *et al.*, An Ultrathin, Smooth and Low-Loss Al-Doped Ag Film and Its Application as a Transparent Electrode in Organic Photovoltaics, *Adv. Mater.*, 2014, **26**, 5696–5701.
146 D. Zhao, C. Zhang, H. Kim and L. J. Guo, High-Performance Ta_2O_5/Al-Doped Ag Electrode for Resonant Light Harvesting in Efficient Organic Solar Cells, *Adv. Energy Mater.*, 2015, **5**, 1500768.
147 M. L. Brongersma, Y. Cui and S. Fan, Light management for photovoltaics using high-index nanostructures, *Nat. Mater.*, 2014, **13**, 451–460.
148 C. Battaglia, J. Escarré, K. Söderström, L. Erni, L. Ding and G. Bugnon, *et al.*, Nanoimprint Lithography for High-Efficiency Thin-Film Silicon Solar Cells, *Nano Lett.*, 2011, **11**, 661–665.
149 K. Wilken, U. W. Paetzold, M. Meier, N. Prager, M. Fahland and F. Finger, *et al.*, Nanoimprint texturing of transparent flexible substrates for improved light management in thin-film solar cells, *Phys. Status Solidi RRL*, 2015, **9**, 215–219.
150 M.-G. Kang, T. Xu, H. J. Park, X. Luo and L. J. Guo, Efficiency Enhancement of Organic Solar Cells Using Transparent Plasmonic Ag Nanowire Electrodes, *Adv. Mater.*, 2010, **22**, 4378–4383.
151 M.-S. Kim, J.-S. Kim, J. Cho, M. Stein, L. J. Guo and J. Kim, Flexible conjugated polymer photovoltaic cells with controlled heterojunctions fabricated using nanoimprint lithography, *Appl. Phys. Lett.*, 2007, **90**, 123113.
152 Y. Yang, K. Mielczarek, A. Zakhidov and W. Hu, Efficient Low Bandgap Polymer Solar Cell with Ordered Heterojunction Defined by Nanoimprint Lithography, *ACS Appl. Mater. Interfaces*, 2014, **6**, 19282–19287.
153 H. S. Youn, H. J. Park and L. J. Guo, Printed Nanostructures for Organic Photovoltaic Cells and Solution-Processed Polymer Light-Emitting Diodes, *Energy Technol.*, 2015, **3**, 340–350.

Published on 18 April 2016. Downloaded by University of Texas Libraries on 14/06/2016 15:37:27.

154 S. H. Ahn and L. J. Guo, Large-Area Roll-to-Roll and Roll-to-Plate Nanoimprint Lithography: A Step toward High-Throughput Application of Continuous Nanoimprinting, *ACS Nano*, 2009, **3**, 2304–2310.

155 T. W. Ebbesen, H. J. Lezec, H. F. Ghaemi, T. Thio and P. A. Wolff, Extraordinary optical transmission through sub-wavelength hole arrays, *Nature*, 1998, **391**, 667–669.

156 N. Fang, H. Lee, C. Sun and X. Zhang, Sub-Diffraction-Limited Optical Imaging with a Silver Superlens, *Science*, 2005, **308**, 534–537.

157 T. Xu, A. Agrawal, M. Abashin, K. J. Chau and H. J. Lezec, All-angle negative refraction and active flat lensing of ultraviolet light, *Nature*, 2013, **497**, 470–474.

158 M. Gharghi, C. Gladden, T. Zentgraf, Y. Liu, X. Yin and J. Valentine, *et al.*, A Carpet Cloak for Visible Light, *Nano Lett.*, 2011, **11**, 2825–2828.

159 X. Ni, Z. J. Wong, M. Mrejen, Y. Wang and X. Zhang, An ultrathin invisibility skin cloak for visible light, *Science*, 2015, **349**, 1310–1314.

160 N. Landy and D. R. Smith, A full-parameter unidirectional metamaterial cloak for microwaves, *Nat. Mater.*, 2013, **12**, 25–28.

161 H. N. S. Krishnamoorthy, Z. Jacob, E. Narimanov, I. Kretzschmar and V. M. Menon, Topological Transitions in Metamaterials, *Science*, 2012, **336**, 205–209.

162 N. Yu, P. Genevet, M. A. Kats, F. Aieta, J.-P. Tetienne and F. Capasso, *et al.*, Light Propagation with Phase Discontinuities: Generalized Laws of Reflection and Refraction, *Science*, 2011, **334**, 333–337.

163 Y.-K. R. Wu, A. E. Hollowell, C. Zhang and L. J. Guo, Angle-Insensitive Structural Colours based on Metallic Nanocavities and Coloured Pixels beyond the Diffraction Limit, *Sci. Rep.*, 2013, **3**, 1194.

164 T. Xu, Y.-K. Wu, X. Luo and L. J. Guo, Plasmonic nanoresonators for high-resolution colour filtering and spectral imaging, *Nat. Commun.*, 2010, **1**, 59.

165 C. Pfeiffer, C. Zhang, V. Ray, L. J. Guo and A. Grbic, High Performance Bianisotropic Metasurfaces: Asymmetric Transmission of Light, *Phys. Rev. Lett.*, 2014, **113**, 023902.

166 J. Y. Chin, T. Steinle, T. Wehlus, D. Dregely, T. Weiss and V. I. Belotelov, *et al.*, Nonreciprocal plasmonics enables giant enhancement of thin-film Faraday rotation, *Nat. Commun.*, 2013, **4**, 1599.

167 A. Melikyan, L. Alloatti, A. Muslija, D. Hillerkuss, P. C. Schindler and J. Li, *et al.*, High-speed plasmonic phase modulators, *Nat. Photonics*, 2014, **8**, 229–233.

168 C. Haffner, W. Heni, Y. Fedoryshyn, J. Niegemann, A. Melikyan and D. L. Elder, *et al.*, All-plasmonic Mach–Zehnder modulator enabling optical high-speed communication at the microscale, *Nat. Photonics*, 2015, **9**, 525–528.

169 B. S. Dennis, M. I. Haftel, D. A. Czaplewski, D. Lopez, G. Blumberg and V. A. Aksyuk, Compact nanomechanical plasmonic phase modulators, *Nat. Photonics*, 2015, **9**, 267–273.

170 D. Franklin, Y. Chen, A. Vazquez-Guardado, S. Modak, J. Boroumand and D. Xu, *et al.*, Polarization-independent actively tunable colour generation on imprinted plasmonic surfaces, *Nat. Commun.*, 2015, **6**, 7337.

171 J. Zhou, A. F. Kaplan, L. Chen and L. J. Guo, Experiment and Theory of the Broadband Absorption by a Tapered Hyperbolic Metamaterial Array, *ACS Photonics*, 2014, **1**, 618–624.

172 B. D. Lucas, J.-S. Kim, C. Chin and L. J. Guo, Nanoimprint Lithography Based Approach for the Fabrication of Large-Area, Uniformly-Oriented Plasmonic Arrays, *Adv. Mater.*, 2008, **20**, 1129–1134.

173 I. Bergmair, B. Dastmalchi, M. Bergmair, A. Saeed, W. Hilber and G. Hesser, *et al.*, Single and multilayer metamaterials fabricated by nanoimprint lithography, *Nanotechnology*, 2011, **22**, 325301.

174 W. Wu, E. Kim, E. Ponizovskaya, Y. Liu, Z. Yu and N. Fang, *et al.*, Optical metamaterials at near and mid-IR range fabricated by nanoimprint lithography, *Appl. Phys. A: Mater. Sci. Process.*, 2007, **87**, 143–150.

175 L. Gao, K. Shigeta, A. Vazquez-Guardado, C. J. Progler, G. R. Bogart and J. A. Rogers, *et al.*, Nanoimprinting Techniques for Large-Area Three-Dimensional Negative Index Metamaterials with Operation in the Visible and Telecom Bands, *ACS Nano*, 2014, **8**, 5535–5542.

176 V. Rinnerbauer, E. Lausecker, F. Schäffler, P. Reininger, G. Strasser and R. D. Geil, *et al.*, Nanoimprinted superlattice metallic photonic crystal as ultraselective solar absorber, *Optica*, 2015, **2**, 743–746.

177 W. Chihhui, N. Burton III, J. Jeremy, M. Andrew, Z. Byron and S. Steve, *et al.*, Metamaterial-based integrated plasmonic absorber/emitter for solar thermo-photovoltaic systems, *J. Opt.*, 2012, **14**, 024005.

178 W. Chen, M. Tymchenko, P. Gopalan, X. Ye, Y. Wu and M. Zhang, *et al.*, Large-Area Nanoimprinted Colloidal Au Nanocrystal-Based Nanoantennas for Ultrathin Polarizing Plasmonic Metasurfaces, *Nano Lett.*, 2015, **15**, 5254–5260.

179 L. Dong, M. J. Haslinger, J. Danzberger, I. Bergmair, K. Hingerl and C. Hrelescu, *et al.*, Giant cross polarization in a nanoimprinted metamaterial combining a fishnet with its Babinet complement, *Opt. Express*, 2015, **23**, 19034–19046.

180 J. K. Hohmann, M. Renner, E. H. Waller and G. von Freymann, Three-Dimensional μ-Printing: An Enabling Technology, *Adv. Opt. Mater.*, 2015, **3**, 1488–1507.

181 J. Fischer and M. Wegener, Three-dimensional optical laser lithography beyond the diffraction limit, *Laser Photonics Rev.*, 2013, **7**, 22–44.

182 K. Sugioka and Y. Cheng, Femtosecond laser three-dimensional micro- and nanofabrication, *Appl. Phys. Rev.*, 2014, **1**, 041303.

183 S. Maruo, O. Nakamura and S. Kawata, Three-dimensional microfabrication with two-photon-absorbed photopolymerization, *Opt. Lett.*, 1997, **22**, 132–134.

184 T. Bückmann, N. Stenger, M. Kadic, J. Kaschke, A. Frölich and T. Kennerknecht, *et al.*, Tailored 3D Mechanical Metamaterials Made by Dip-in Direct-Laser-Writing Optical Lithography, *Adv. Mater.*, 2012, **24**, 2710–2714.

 This journal is © The Royal Society of Chemistry 2016

Published on 18 April 2016. Downloaded by University of Texas Libraries on 14/06/2016 15:37:27.

185 B. Tiemo, S. Robert, T. Michael, K. Muamer, W. M. Graeme and W. Martin, On three-dimensional dilational elastic metamaterials, *New J. Phys.*, 2014, **16**, 033032.
186 S. W. Hell and J. Wichmann, Breaking the diffraction resolution limit by stimulated emission: stimulated-emission-depletion fluorescence microscopy, *Opt. Lett.*, 1994, **19**, 780–782.
187 J. Fischer and M. Wegener, Three-dimensional direct laser writing inspired by stimulated-emission-depletion microscopy [Invited], *Opt. Mater. Express*, 2011, **1**, 614–624.
188 G. Vizsnyiczai, L. Kelemen and P. Ormos, Holographic multi-focus 3D two-photon polymerization with real-time calculated holograms, *Opt. Express*, 2014, **22**, 24217–24223.
189 K. Obata, J. Koch, U. Hinze and B. N. Chichkov, Multi-focus two-photon polymerization technique based on individually controlled phase modulation, *Opt. Express*, 2010, **18**, 17193–17200.
190 M. T. Do, T. T. N. Nguyen, Q. Li, H. Benisty, I. Ledoux-Rak and N. D. Lai, Submicrometer 3D structures fabrication enabled by one-photon absorption direct laser writing, *Opt. Express*, 2013, **21**, 20964–20973.
191 P. Mueller, M. Thiel and M. Wegener, 3D direct laser writing using a 405 nm diode laser, *Opt. Lett.*, 2014, **39**, 6847–6850.
192 J. K. Gansel, M. Thiel, M. S. Rill, M. Decker, K. Bade and V. Saile, *et al.*, Gold Helix Photonic Metamaterial as Broadband Circular Polarizer, *Science*, 2009, **325**, 1513–1515.
193 J. L. Digaum, J. J. Pazos, J. Chiles, J. D'Archangel, G. Padilla and A. Tatulian, *et al.*, Tight control of light beams in photonic crystals with spatially-variant lattice orientation, *Opt. Express*, 2014, **22**, 25788–25804.
194 N. Lindenmann, G. Balthasar, D. Hillerkuss, R. Schmogrow, M. Jordan and J. Leuthold, *et al.*, Photonic wire bonding: a novel concept for chip-scale interconnects, *Opt. Express*, 2012, **20**, 17667–17677.
195 M. Schumann, T. Buckmann, N. Gruhler, M. Wegener and W. Pernice, Hybrid 2D–3D optical devices for integrated optics by direct laser writing, *Light: Sci. Appl.*, 2014, **3**, e175.
196 H. Zhang, N. A. Amro, S. Disawal, R. Elghanian, R. Shile and J. Fragala, High-Throughput Dip-Pen-Nanolithography-Based Fabrication of Si Nanostructures, *Small*, 2007, **3**, 81–85.
197 P. Rath, M. Hirtz, G. Lewes-Malandrakis, D. Brink, C. Nebel and W. H. P. Pernice, Diamond Nanophotonic Circuits Functionalized by Dip-pen Nanolithography, *Adv. Opt. Mater.*, 2015, **3**, 328–335.
198 C. Pina-Hernandez, L. J. Guo and P.-F. Fu, High Resolution Functional Epoxysilsesquioxane-Based Patterning Layers for Large Area Nanoimprinting, *ACS Nano*, 2010, **4**, 4776–4784.